Relating Topology and Dynamics
in Neuronal Networks

31 March 2010

Master's Thesis

in partial fulfilment

of the requirements for the degree "Master of Science"

in the Neuroscience Programme

at the Georg August University Göttingen, Faculty of Biology

submitted by

Gorur Shandilya Srinivas

born in

Vellore, India

Declaration

Herewith I declare, that I prepared the Master's Thesis "The Topology and Dynamics of Neuronal Networks" on my own and with no other sources and aids than quoted.

Contents

List of Figures

List of Tables

Acknowledgements

Abstract

Understanding the core interconnections between network structure and dynamics is an essential step towards understanding brain function. Recent work has revealed tantalising sketches of a class of principles governing the interplay between network dynamics and topology. Experimental and numerical work on the Stomatogastric Ganglion (STG) of the lobster has shown that a large, heterogeneous set of distinct three-neuron networks can exhibit similar collective dynamics, despite significant differences in network topology and neuron parameters. Complementarily, theoretical work has shown that the dynamics of networks of leaky integrate-and-fire (LIF) neurons restricts the space of possible networks onto a lower-dimensional manifold in the space of network topologies. Here, I present numerical results that suggest that dynamics restricts permissible topology even for a biophysically-detailed model of the STG network. These results reveal that the dynamical behaviour of the STG network is robust to changes in network structure in some topological dimensions, but fragile in other dimensions. Further, I describe different kinds of transitions from networks with canonical dynamics to unorthodox networks with different dynamical metrics, on moving through parameter space. The existence of these transitions provides further evidence for the presence of a high-dimensional manifold on which all networks dynamically identical to the canonical STG network lie. To disentangle the effects of network topology from the complexity of the neuron model, I study a simplification of this network based on the Kuramoto Model. Using this simplified model, I demonstrate a method to reconstruct the effective coupling strengths between neurons in a network by inducing small perturbations to the limit cycle of the network.

1   Introduction

"There is nothing new to be discovered in physics now. All that remains
is more and more precise measurement" — attributed to Lord Kelvin [42]

1.1   Background

The Physics of the last century rests on two complementary processes: the toolbox of
analysis, that equips the physical scientist to describe a system mathematically, and
the framework of models, that allows her to understand the mechanisms underlying
observable behaviour. In Mechanics, this allowed for the development of analytical
tools that help predict how mechanical systems of known structure might behave.
Conversely, modelling facilitated the construction of a set of plausible hypothesis of the
constituents and function of a system, readily verifiable by experiment, and suggested
causal relationships between observable behavior and underlying mechanisms.

The Physics of our human-scale world is powerful enough, through analysis, to pre-
dict the behavior of a mechanical system of arbitrary structure. Through modelling,
it's possible to predict the structure of a system from an arbitrary behavioral observa-
tion. Where classical physics fails, and thus, where current research is focused, is in
the 'very large, the very small and the very complex' [1]. Some of the most interesting
areas of current research in 'the very complex' are in the study of networks.

In contrast to the established success of physical theory in classical mechanics,
'Network Science' is in its infancy [2]. Networks are often studied as mathematical
objects called 'graphs'. A graph is a collection of nodes, called vertices, and links
between these nodes, called 'edges' [17]. An edge may be directed or undirected, and
may have a weight, or strength [18, 10].

There is currently no fundamental theory that predicts the behavior of a dynam-
ical system on a network of arbitrary topology, nor is there a framework mediating
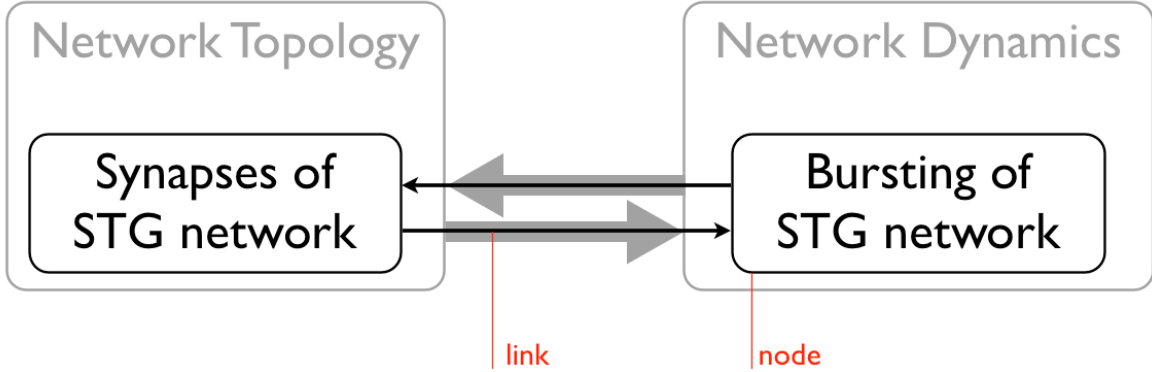
Figure 1: **Outline and Definitions. This study aims to reveal causal links from the topology of networks to their dynamics, and mechanistic links from the dynamics of networks to their structure. This mathematical structure is a 'graph', consisting of nodes, or 'vertices' connected by links, or 'edges'.**

the relationship of classes of behavior a network exhibits to the structure it needs to generate the behavior.

This is partly because networks are inherently difficult to understand, as can be seen from Steven Strogatz's list of potential complications with networks [41]:

1. **Structural complexity:** the connections between the nodes of a network can be very complex. A neuronal cell in your brain may have up to 10^4 synapses with other neurons [36], and brain architecture at the inter-cellular level is so complex that little is known about it.

2. **Network evolution:** these connections can change over time. As you read this sentence, connections are being made, broken or modified— some irreversibly— between neurons in your brain.

3. **Connection diversity:** the 'edges' between nodes can have different weights, directions and signs, or can be of different kinds. Synapses between neurons can be strong or weak, inhibitory or excitatory, or can be electrical or chemical.

4. **Dynamical complexity:** the nodes can be nonlinear dynamical systems. In the network presented in this study, each node is a 13-dimensional nonlinear system with rich intrinsic dynamical behaviour.

5. **Node diversity:** there could be many different kinds of nodes. Though the network presented here has only three nodes (neurons), they are all different.

As can be seen from these illustrative examples, neuronal networks are an intriguing class of networks, displaying all the complexities inherent to networks. Neuroscience offers some the most exciting problems in networks. Networks of neurons act on astonishingly small time scales to process and store information, and are themselves shaped by evolutionary processes on much larger time scales. Thus, while a fairly detailed understanding of the structure and behavior of individual nodes of the network— the neurons— has been achieved [59], this has not substantially contributed to our understanding of large neuronal networks like the brain, because a very large number of neurons ($\approx 10^{10}$) interact in extremely complex ways to produce collective dynamical states that are poorly understood.

Thus, a good theory of brain function requires a good theory of networks.

1.2   Goals and Outline

The broad goal of this study is to link network topology and network behaviour, formulated in two complementary questions: how does the topology of a network affect its dynamical behaviour, and, conversely, given the dynamical behaviour of a network, what can be said of its underlying structure? This thesis is structured around these two questions.

The first question: how does network structure affect its dynamical behaviour? Here, it is important to acknowledge that universalisms from network structure to dynamics may not exist — the fine details of the dynamical system running on the network *do* matter [41]. The dynamical behaviour of a network is a concatenation of both network topology and details concerning the dynamics of nodes, as well as a host of other parameters, like those governing interactions between nodes.

A significant contribution towards answering this question was made by Prinz, Bucher and Marder. In a paper published in 2004, the authors show that similar network activity can arise from a very heterogeneous set of networks with disparate topologies and neuron parameters [32]. They demonstrate this for a three-neuron model of the lobster Stomatogastric Ganglion (STG). The lobster STG is a small central pattern generator that generates a characteristic triphasic bursting motor pattern (Fig. 3). Unlike many other experimentally accessible networks, whose connectivity is largely unknown, the connections between the neurons in this networks is known [32].

The model consists of three neurons, each of a different type. By simulating $\approx 2\mathrm{x}10^{7}$ STG networks with different topological and neuronal parameters, and by parameter-
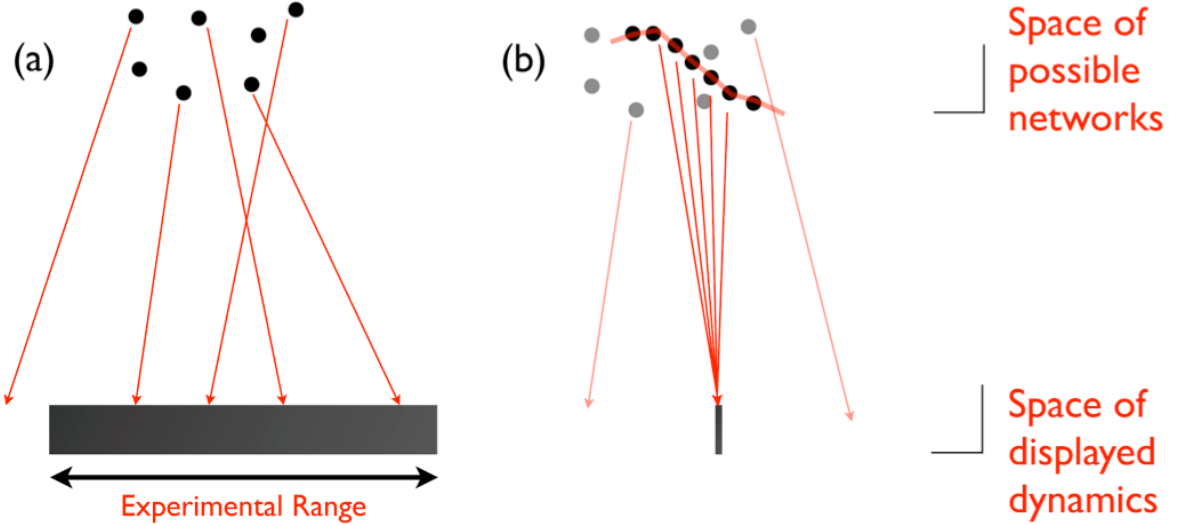
Figure 2: **Comparison of the objectives of this thesis to that of Prinz et. al. (a) Prinz et. al. coarsely sample the space of possible networks, identifying networks that exhibit behaviour within some region of allowed behaviour. (b) This study searches for a manifold within the space of possible networks, such that every point (network) on that manifold displays a single behaviour.**

ising the observed dynamical behaviour, the authors show that a large, heterogeneous set of networks produces a bursting pattern indistinguishable from experimentally observable pyloric rhythms (See Figure 2).

The STG model neuron is described in Section 2.1, and the STG model network in Section 2.2. Using the STG network, Section 3 will detail the central result of this thesis: that the large, heterogeneous set of networks described by Prinz, Bucher and Marder isn't merely a collection of oddballs, but instead lie on a high-dimensional manifold of *all* such dynamically-identical networks. In conjunction with theoretical work on linear-integrate-and-fire (LIF) networks, where the existence of this manifold has been shown [8], the results presented in this thesis suggest that a generic network exhibiting some dynamical behaviour coexists, with all other dynamically-identical networks, on a manifold in the space of network topologies. The implications of these findings on are explored in Section 3.4.2.

Secondly, what constraints does the behaviour of a network impose on the its structure? Knowing the behaviour of a network, can we infer its structure? In Section 4, it will be shown that constraints *can* be imposed on the space of network topologies by its response dynamics. A theory of network reconstruction based on perturbation analysis is introduced, and applied to networks of phase-coupled Kuramoto oscillators and the lobster Stomatogastric Ganglion (STG).

1.2   Goals and Outline

The models used for the network of Kuramoto oscillators and the STG network are described in Section 2. Following the failure to reproduce published results on the STG network, a detailed analysis of the effects of choice of solver for the neuron model is presented in Section 6.1. Further, the periodicity of the STG neuron model is investigated in Section 6.2.

2 Models

"No insight is gained if the model is as perplexing as the phenomena it is supposed to describe. This is what makes mathematical modelling an art as well as a science: An elegant model strikes just the right compromise between simplicity and verisimilitude" — Steven Strogatz [50]

In this section, the neuron and network models used in this study are presented. After the description of the STG neuron model in the following subsection, three of these neuron models are 'wired together' with seven synapses, detailed in Section 2.2. The neuron models are dynamically identical, differing solely in one set of parameters, i.e., their maximal membrane conductances. Thus the description of the STG network adds to the neuron model only synaptic dynamics and parameters, and the neuron parameters themselves, listed in Table 2. Finally, the Kuramoto Model of phase-coupled oscillators is briefly described in Section 2.3.

2.1 The STG Neuron Model

The neuron model used in this study is a 13-dimensional electronically compact, conductance based model [35]. This model is considered bio-physically detailed in that several ionic currents are modelled, as is the intracellular calcium concentration. This model was developed to faithfully replicate the bursting oscillatory nature of the neurons in the STG network, and is based on experimental data obtained from lobster Stomatogastric neurons [44], as described in detail in [5].

Each of the model's membrane currents is described by

$$I_i = g_i m_i^p h_i \left(V - E_i \right) A \tag{1}$$

where $A = 0.6238 \times 10^{-3} cm^2$ is the membrane area, E_i is the reversal potential, and g_i is the maximal conductance of the ith ionic current. The reversal potentials are 50 mV for Na$^+$, 80 mV for K$^+$, 20 mV for I_H and 50 mV for I_{leak}. The reversal potential for the Ca^{2+} currents are determined from the instantaneous intracellular Ca^{2+} concentrations using the Nernst Equation:

$$E_i = \frac{RT}{nF} \ln \frac{[Ca^{2+}]_{outside}}{[Ca^{2+}]_{inside}} \tag{2}$$

where $[Ca^{2+}]_{outside} = 3$mM. The activation and inactivation variables m_i and h_i change according to

$$\dot{m}_i = \frac{m_\infty - m_i}{\tau_m} \quad \text{and} \quad \dot{h}_i = \frac{h_\infty - h_i}{\tau_h} \tag{3}$$

where $m_\infty, h_\infty, \tau_m$ and τ_h, along with the exponents p_i are given in Table 1.

The membrane potential is governed by

$$\dot{V} = \frac{\sum_i I_i}{C} \tag{4}$$

where $C = 0.628$nF is the capacitance of the neuron. The rate of change of intracellular calcium concentration

$$\frac{d[Ca^{2+}]}{dt} = \frac{-f(I_{CaT} + I_{CaS}) - [Ca^{2+}] + [Ca^{2+}]_0}{\tau_{Ca}} \tag{5}$$

where $\tau_{Ca} = 200$ms is the Ca^{2+} buffering time constant, f $= 14.96$M/nA maps the Calcium current onto an intracellular concentration change [4], and $[Ca^{2+}]_0 = 0.05$M is the steady-state intracellular Calcium concentration. Together, these thirteen coupled differential equations (1-5) fully describe the dynamics of the neuron model.

These differential equations comprise a 'stiff' problem. A stiff set of equations is a set of differential equations which is prone to numerical instabilities, when solved by some numerical solvers, unless the step size is extremely small. In these equations, the 'stiffness' of these equations is manifest in the very different timescales of action: while intracellular concentration oscillates on a time scale of around one second, the gating variables for some channels, and the membrane potential, can oscillate on a millisecond time scale, e.g., during an action potential. Special methods are advisable to solve stiff equations, like the Shampine-Reichelt-Kierzenka trapezoidal rule using
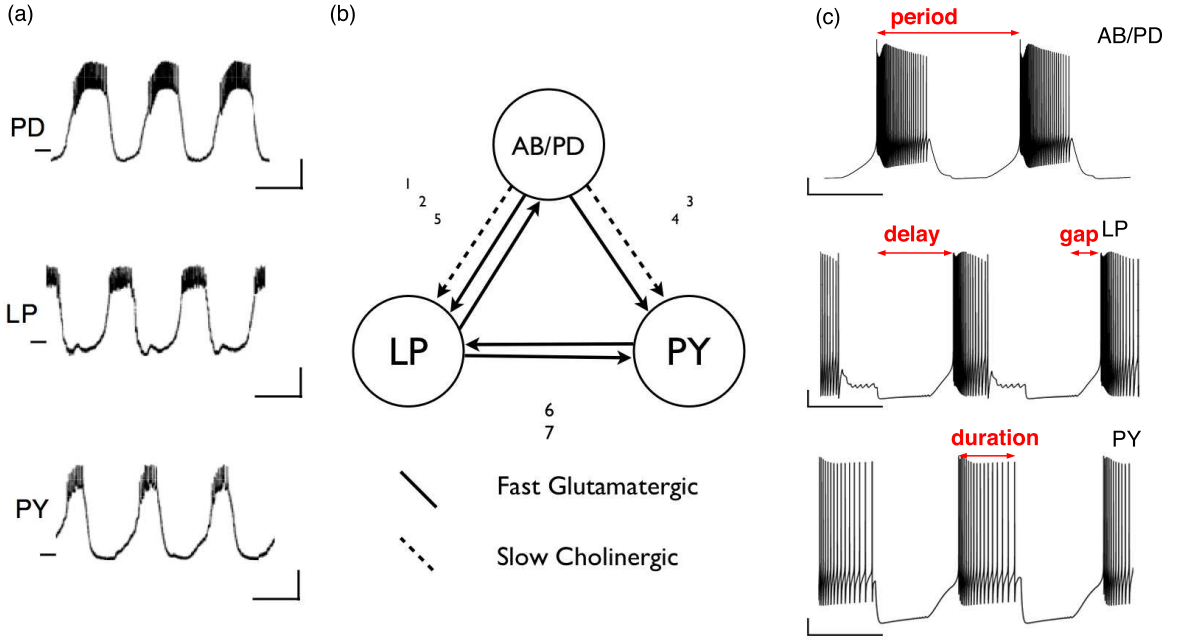
Figure 3: **(a) Pyloric rhythm recorded from *H. americanus* with intracellular electrodes. Adapted from [32]. The canonical behaviour of the pyloric network is a triphasic rhythm with bursts occurring in the order PD-LP-PY. (b) Graph representation of a simplified version of the STG circuit. All synapses in the circuit are inhibitory. (c) Voltage traces from the model described in the text. Vertical scale bars 10mV, horizontal scale bars 1s. Horizontal lines are at -60mV. Definition of the four metrics (period, delay, gap, duration) used to characterise plyoric bursts (red).**

free interpolants [39].

However, to conform to the to the methodology used in previous work [35, 32, 5], the equations for the gating variables were integrated using the first-order Euler method, and the equations for the membrane potential and the intracellular calcium concentration were integrated with the exponential method described in Dayan and Abbott [36].

An analysis on the various solvers (See Section 6.1 for a detailed presentation) revealed that (1) the behaviour of certain neuron models in [32] could not be reproduced (2) the exponential Euler method described in [36] produced the ideal compromise between speed and precision. Thus, all simulations presented here were produced by the exponential Euler method, with a fixed time step of 50μs unless otherwise specified.

The neuron models in isolation cover a full spectrum of dynamic behaviours, from complete silence to regular spiking to periodic bursting. In general, AB/PD neurons burst spontaneously, and induce phase-locked bursting in LP or PY neurons by post-

inhibitory rebounds [32].

2.2   The STG Network Model

The lobster STG is a small central pattern generator that generates a characteristic triphasic bursting motor pattern (Fig. 3). In its simplest form, the pyloric rhythm is produced by a pacemaker kernel consisting of the anterior burster (AB) neuron, which is electrically coupled to two pyloric dilator (PD) neurons, and of two other neurons types: a single lateral pyloric (LP) neuron and five to eight pyloric (PY) neurons [43]. The LP and PY neurons receive inhibitory glutamatergic synapses with fast dynamics from the AB neuron, and inhibitory cholinergic synapses with slow dynamics from the PD neurons [32]. The LP neuron feeds back to the PD neuron via an inhibitory glutamatergic synapse. There are some reciprocal inhibitory connections between the LP neuron and the PY neurons. All synapses in the STG are inhibitory.

The STG network is unique in the fact that it is a functional biological network of known connectivity and stereotyped behaviour. Detailed bio-physically realistic models of the STG network have been constructed [35, 32, 5] that effectively mimic experimental observations. The model STG network is constructed according to Figure 3. All simulations assumed the neuron parameters given in Table 2. This choice corresponds to neurons AB/PD#2, LP#4, PY#1, and the resulting network is labelled (e) in Figure 3 in [32].

As previously mentioned, all three neurons are dynamically identical, differing only in membrane conductance parameters (See Table 2). Thus, the specification of the STG network dynamics now requires a specification of the synaptic dynamics to be complete.

All synapses were simulated according to an established model of synaptic dynamics [45]. The synaptic current is

$$I_s = g_s s \left(V_{post} - E_s \right) \tag{6}$$

where g_s is the maximal synapse conductance, V_{post} is the membrane potential of the post-synaptic neuron and E_s is the reversal potential of the synapse. The dynamics of the activation variable s is given by

$$\dot{s} = \frac{\bar{s} \left(V_{pre} - s \right)}{\tau_s} \tag{7}$$

Table 1: **Voltage Dependence of Model Currents. The time constants τ_m and τ_h are in milliseconds, V is in millivolts, and the intracellular Calcium concentration is in μM. m_∞, h_∞ and *p* are dimensionless**

	p	m_∞	h_∞	τ_m	τ_h
I_{Na}	3	$\dfrac{1}{1+\exp\left(\frac{V+25.5}{-5.29}\right)}$	$\dfrac{1}{1+\exp\left(\frac{V+48.9}{5.18}\right)}$	$2.64-\dfrac{2.52}{1+\exp\left(\frac{V+120.0}{-25.0}\right)}$	$\dfrac{1.34}{1+\exp\left(\frac{V+62.9}{-10}\right)}\left[1.5+\dfrac{1}{1+\exp\left(\frac{V+34.9}{3.6}\right)}\right]$
I_{CaT}	3	$\dfrac{1}{1+\exp\left(\frac{V+27.1}{-7.2}\right)}$	$\dfrac{1}{1+\exp\left(\frac{V+32.1}{5.5}\right)}$	$43.4-\dfrac{42.6}{1+\exp\left(\frac{V+68.1}{-20.5}\right)}$	$210.0-\dfrac{179.6}{1+\exp\left(\frac{V+55.0}{-16.9}\right)}$
I_{CaS}	3	$\dfrac{1}{1+\exp\left(\frac{V+33.0}{-8.1}\right)}$	$\dfrac{1}{1+\exp\left(\frac{V+60.0}{6.2}\right)}$	$2.8+\dfrac{14.0}{\exp\left(\frac{V+27.0}{10.0}\right)+\exp\left(\frac{V+70.0}{-13.0}\right)}$	$120+\dfrac{300}{\exp\left(\frac{V+55.0}{9.0}\right)+\exp\left(\frac{V+65.0}{-16.0}\right)}$
I_A	3	$\dfrac{1}{1+\exp\left(\frac{V+27.2}{-8.7}\right)}$	$\dfrac{1}{1+\exp\left(\frac{V+56.9}{4.9}\right)}$	$2.32-\dfrac{20.8}{1+\exp\left(\frac{V+32.9}{-15.2}\right)}$	$77.2-\dfrac{58.4}{1+\exp\left(\frac{V+38.9}{-26.5}\right)}$
I_{KCa}	4	$\dfrac{[Ca^{2+}]}{[Ca^{2+}]+3}\left[\dfrac{1}{1+\exp\left(\frac{V+28.3}{-12.6}\right)}\right]$		$180.6-\dfrac{150.2}{1+\exp\left(\frac{V+46.0}{-22.7}\right)}$	
I_{Kd}	4	$\dfrac{1}{1+\exp\left(\frac{V+12.3}{-11.8}\right)}$		$14.4-\dfrac{12.8}{1+\exp\left(\frac{V+28.3}{-19.2}\right)}$	
I_H	1	$\dfrac{1}{1+\exp\left(\frac{V+75.0}{5.5}\right)}$		$\dfrac{2.0}{\exp\left(\frac{V+169.0}{-11.6}\right)+\exp\left(\frac{V-26.7}{14.3}\right)}$	

where

$$\bar{s}\left(V_{pre}\right) = \frac{1}{1 + \exp\left(\dfrac{V_{th} - V_{pre}}{\Delta}\right)} \quad \text{and} \quad \tau_s = \frac{1 - \bar{s}\left(V_{pre}\right)}{k_-} \tag{8}$$

where V_{pre} is the membrane potential of the pre-synaptic neuron, V_{th} is the threshold voltage of the synapse, Δ determines the slope of the activation curve and k_- is the rate constant for the rate of transmitter-receptor dissociation. AB, LP and PY are glutamatergic neurons, whereas PD is cholinergic [48, 46, 47]. Thus, even though the electrical coupling between AB and PD is modelled by collapsing them into a common AB/PD neuron, their output is modelled individually due to their non-identical synaptic dynamics. The modelling of AB and PD by a single neuron neglects the time constants of the electrical coupling between them, which, given their large membrane capacitance, is significant. However, this provides a major simplification of the STG network at a relatively small cost.

For glutamatergic synapses, $E_s = 70$mV and $k_- = 1/40$ ms, and for cholinergic synapses $E_s = -80$ mV and $k_- = 1/100$ ms. For both synapse types, $V_{th} = -35$ mV and $\Delta = 5$ mV. These parameters are chosen to capture, to a first approximation, the slow dynamics of cholinergic inhibitory post-synaptic potentials (IPSPs) and the fast dynamics of glutamatergic IPSPs [49].

The maximal synapse conductance g_s is taken to be a measure of the synapse strength.

This model was initialised from a fixed initial condition specified in the STG model neuron database [5]. The synaptic dynamical variables were set to 0. During each simulation, the system was allowed to evolve for five seconds before observations were made, in an attempt to free the observed dynamical behaviour of transient artefacts.

Simulations were written in the MATLAB language and complied binaries were run on a varying number of AMD Opteron processors, each clocked at 2.4 GHz. The mean speed of code execution at a temporal resolution of 50μs was about 20% realtime.

2.3   The Kuramoto Model

The Kuramoto model, first proposed by Yoshiki Kuramoto [34, 26], is a mathematical model of a network of phase coupled oscillators. The model is a good approximation

Table 2: **Neuron Parameters: Maximal Membrane Conductance Densities, in mS/cm^2 for the three neurons in the STG network**

	g(I_{Na})	g(I_{CaT})	g(I_{CaS})	g(I_A)	g($I_{K(Ca)}$)	g(I_{Kd})	g(I_H)	g(I_{leak})
AB/PD	100	2.5	6	50	10	100	0.01	0
LP	100	0	4	20	0	25	0.05	0.03
PY	100	2.5	2	50	0	125	0.05	0

for weakly coupled limit-cycle oscillators. This means that the time scales of motion towards the limit cycle of each oscillator is far smaller than the time scale of the oscillation itself.

This model describes a system of oscillators exhibiting two dynamics: an intrinsic oscillatory dynamics specified by the intrinsic frequency of each oscillator, and a collective dynamics specified by the interactions of each oscillator with its neighbours. The interactions are specified by coupling functions *f*, that are smooth and continuously differentiable, and operate on the phases of the oscillators. The oscillators are located on the nodes of a directed graph, and the presence of an edge between node i and node j allows an interaction between the two oscillators. Thus, the rate of change of the phase of each oscillator can be expressed as

$$\dot{\phi}_i = \omega_0 + \sum_{j=1}^{N} J_{ij} f(\phi_i - \phi_j) \tag{9}$$

where ω_0 is the intrinsic frequency of each oscillator and J_{ij} is the coupling constant between i and j. In general, strongly connected networks with weak positive coupling synchronise [26]. For inhibitory couplings, where $J_{ij} < 0$ for all i, j, the system does not synchronise but approaches a phase locked state characterised by *N-1* independent phase differences and a collective frequency Ω_0 that is, in general, different from ω_0.

Despite the fact that the Kuramoto Model is a one-dimensional, phase coupled system, it provides a useful simplification of the STG network. Though the STG network communicates via action potentials, in its functional state, the bursting nature of all neurons depreciates the significance of each spike. Furthermore, each neuron behaves like an oscillator for the STG network in its functional state. The intracellular Calcium concentration rises nearly monotonically in each period, and a meaningful phase can be extracted from it. Moreover, by mutual inhibitory coupling, the STG network in its functional state achieves the 'target' pyloric rhythm, which can be meaningfully mea-

sured by two phase differences. A network of three Kuramoto oscillators with negative coupling whose coupling strengths approximate that of the STG network settles into a phase locked stable orbit characterised by two independent phase differences.

3 From Topology to Dynamics

"The greatest challenge today, not just in cell biology and ecology but in all of science, is the accurate and complete description of complex systems. Scientists have broken down many kinds of systems. They think they know most of the elements and forces. The next task is to reassemble them, at least in mathematical models that capture the key properties of the entire ensembles." — E.O. Wilson [40, 41]

The subject of this section is how a network's topology affects its emergent dynamics. A brief review of current research describes some general themes in high-dimensional dynamical systems, like fragile-yet-robust behaviour, and the interplay between microscopic parameters and global dynamics. Section 3.2 presents a simple *gedankenexperiment*, offering a deeper understanding of the structure of maps from topology to dynamics of networks. The central results of this thesis are presented in Section 3.4, offering evidence in support of the hypotheses made in Section 3.2.

3.1 What would a Network do?

In their 2004 paper, Prinz, Bucher and Marder [32] show that a very large number of networks with different neuron parameters and network topology can exhibit a functionally relevant pyloric rhythm. By simulating $\approx 2\mathrm{x}10^7$ networks coarsely spanning the seven dimensional parameter-space of network topology and a subset of neuron parameters, they show that a large number of networks ($\approx 2.2\%$) show dynamical behaviour very similar to experimentally observed behaviour (See Figure 2). They suggest that cellular and synaptic properties do not need to be tuned to achieve a target network dynamic. Further, they posit that the collective dynamics of a network may be more tightly regulated than lower-level parameters.

Intriguingly, this theme is present in other high-dimensional systems, even in individual neurons. Elliot et. al. [6] discriminate between how a sensory neuron's preferred operating point is set and how its preferred operating point is maintained through adaptation. They then suggest that a neuron varies its operating point such that it keeps the probability density function of its output spike train invariant.
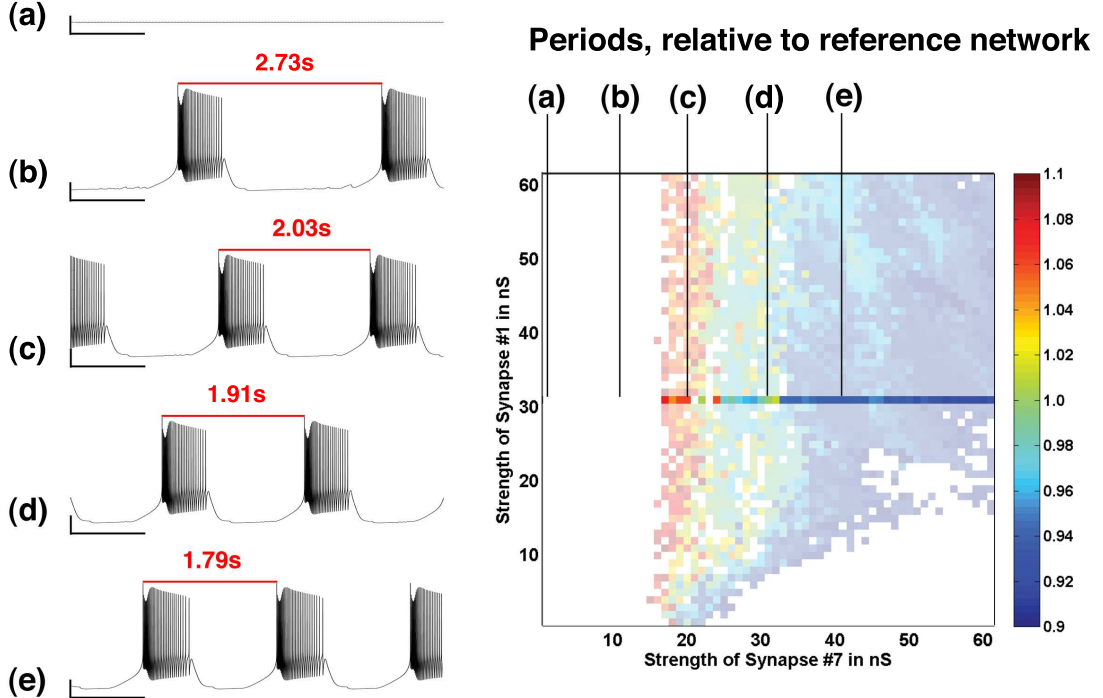
Figure 4: **Construction of colourmaps of the parameter planes. Pairs of synapses are varied and the metrics are computed from voltage traces. Voltage traces of AB/PD (a-e) show different behaviours, from silence, to slow bursting to rapid bursting. The periods are shown in red. The voltage traces are from values of Synapse # 7 of 0, 10,19,30 and 40 nS, with all other synapses maintained at their default strengths. The location of the voltage traces is shown on the colourmap on the right. The line corresponding to a strength of 30nS for Synapse # 1 has been highlighted for clarity.**

Goldman, Marder and Abbott [16] show that a neuron's behaviour is robust in some dimensions of parameter space, and fragile in others. Specifically, for a five-dimensional neuron model, they explored its stability properties over a space of parameters spanning neuromodulator action and conductance. They found slab-shaped regions of uniform behaviour in this parameter space, such that moving parallel to the slab, equivalent to a conductance shift, results in little change, and thus leads to its stability; and moving perpendicular to the slab, an operation corresponding to the effect of neuromodulators,

leads to a dramatic change in the behaviour of the neuron.

Liu et. al. [4] address a similar problem when they introduce a model neuron that tries to capture how real neurons have stationary activity despite rapid channel turnover. They realise this process in a model where maximal conductances are allowed to be controlled by three independent Calcium-driven feedback loops. They show that perturbations to the steady state behaviour in this model cause an exponential relaxation to a new state. On removing the perturbation, the system shifts to a new state whose macroscopic properties are identical to the unperturbed state, but whose microscopic states are distinct from those prior to the perturbation.

At a network level, Prinz et. al. [35] performed experiments where 'artificial synaptic conductance' pulses were injected into neurons. These pulses are defined by an amplitude, corresponding to a synaptic strength, and a duration. They find that while the phase response properties of a neuron changed in both dimensions, the response properties saturate in the amplitude dimension, in contrast to the duration dimension, where neuronal responses do not saturate. They identify the cause of this saturation in their neuron model: inward currents at hyper-polarised potentials. Thus, saturated responses suggest that changes in network topology are not always relevant, and that these changes may have no further impact on network dynamics.

3.2 A Dynamical Systems Perspective

As with other cutting-edge research, the studies listed above have led to a large number of open questions. Firstly, given that a wide variability exists in the dynamics of the STG and other central-pattern generators, it is unclear if animal-to-animal variability in network dynamics is a consequence or cause of regulation of sub-network elements [15]. Secondly, while Prinz et. al. have shown [32] the existence of a large number of networks that show pyloric behaviour, it is possible that this set is merely a set of exceptions, implying that synapse parameters have to be 'tuned' to achieve a target dynamic behaviour.

A simple *gedankenexperiment* puts the problem on a more formal footing. An STG network N characterised by the set of weights of its seven synapses s_0, exhibits a characteristic asymptotic behaviour, that can be defined by a few metrics like the period, delay, gap and duration (see Figure 3 for definitions) x_0. Then, one of the following is true:

1. The neighbourhood of the point s_0 in the seven-dimensional space of synaptic

strengths is the only set where N exhibits behaviour x_0.

2. N exhibits behaviour x_0 in a number of isolated points in parameter space.

3. N exhibits behaviour x_0 in a manifold within this seven-dimensional space.

If (1) or (2) is true, then synaptic strengths have to be under very tight regulation to achieve a target dynamic behaviour. However, there is reason to consider (3) over the others. Firstly, Prinz et. al. [32] search the seven dimensional parameter space of synaptic strengths at discrete strengths: 0nS, 1nS, 3nS, 10nS, 30 nS, and 100 nS. Since these strengths are arbitrarily chosen, it is likely that an equally large number of pyloric-networks are found with a different sampling of parameter space, suggesting that tight regulation of synaptic strengths is not necessary for realising a target dynamic behaviour.

The second argument's intuitive nature sheds further light on the previous result. Given that the space of parameters that a network is allowed to vary in, is higher dimensional than the space of metrics used to quantify its behaviour, the mapping from the high-dimensional set of networks to the low-dimensional set of dynamical behaviours is generically many-to-one. A many-to-one mapping naturally precludes (1).

Certain qualifiers apply here: for the purpose of this argument, both spaces are assumed to be sampled at an equal number of discrete points, and have the same 'extent'. Behaviors not falling directly onto sampling points in behaviour-space are rounded to the nearest point. This corresponds to a finite tolerance in error in the original study [32].[1]

The strongest argument for (3) comes from recent theoretical work on networks of spiking linear-integrate-and-fire (LIF) neurons [8, 9]. The authors, Memmesheimer and Timme, demonstrate that imposing a predefined spike pattern restricts the set of permissible networks in a well-defined manner. For LIF networks, and for most spike patterns, they show analytically that the space of permissible networks is restricted to a lower dimensional manifold within the *N(N-1)* space of network parameters.

---

[1]Prinz et. al. define 'pyloric' networks as those where 15 metrics of behaviour are within the experimental range, i.e., within two standard deviations of the experimental mean.
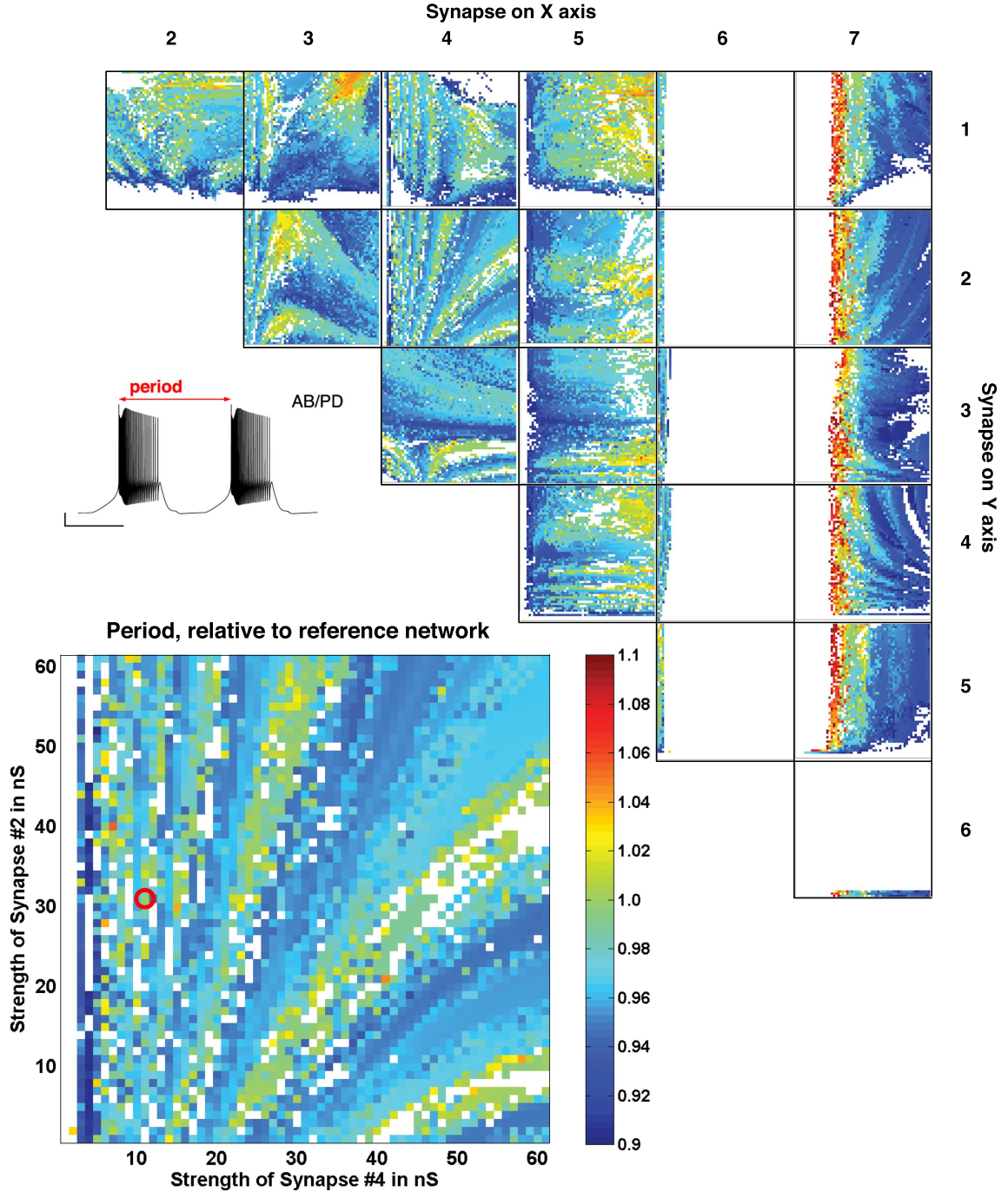
Figure 5: **Colourmaps of the ratios of periods of 78,141 networks to the period of the reference network (red circle in magnified colourmap). These networks lie on planes in the space of synaptic strengths, bounded by 0nS and 60nS. In every colourmap, green corresponds to 1. White areas are networks with unorthodox dynamics. The strength of the synapse is expressed by g_s in Equation (6). The magnified colourmap shows the accordion transition described in Section 3.4, with alternating bands of networks with canonical dynamics (green) and unorthodox dynamics (blue).**

27
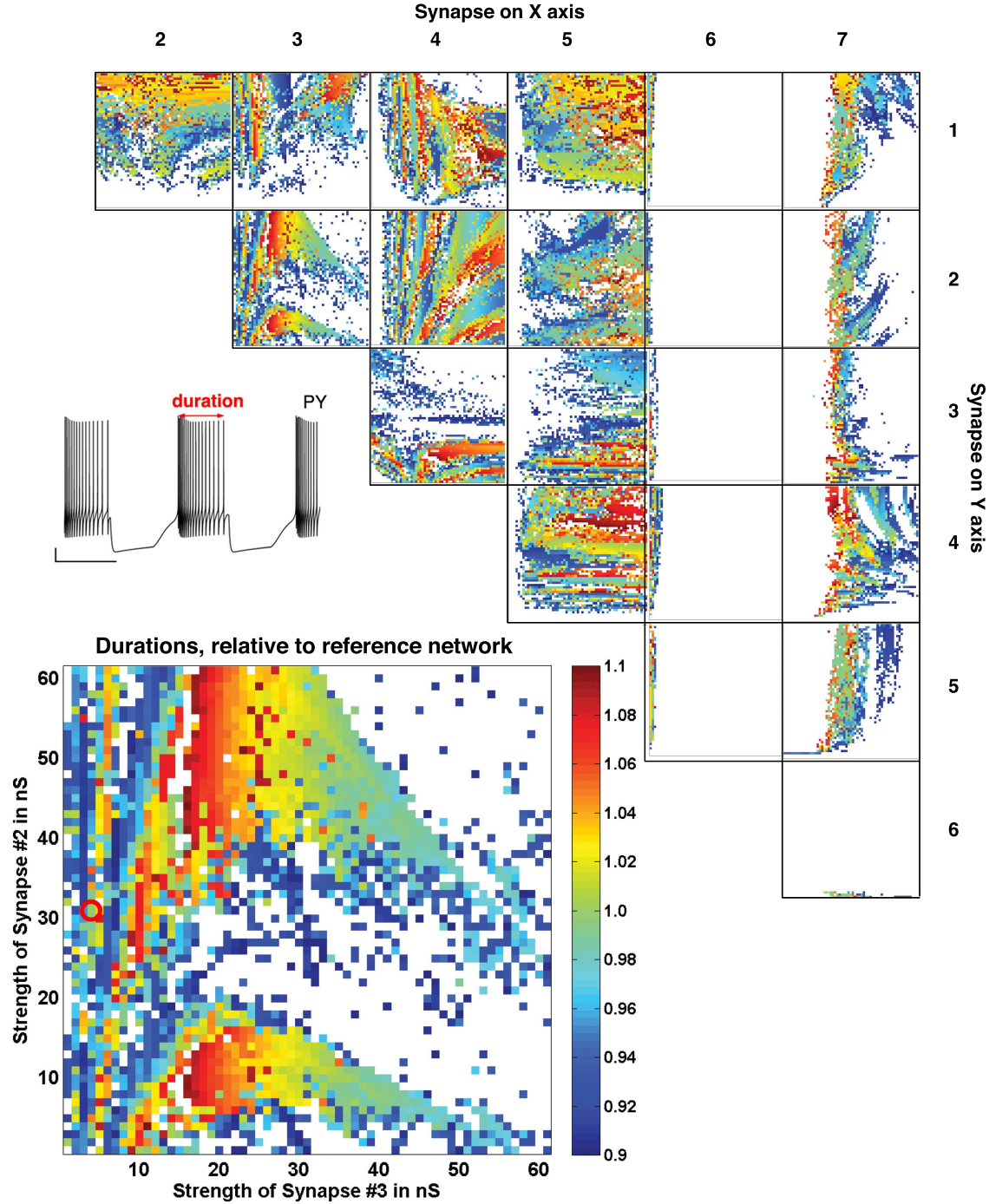
Figure 6: **Colour maps of the ratios of durations of 78,141 networks to the duration of the reference network (red circle). All colourmaps as in Figure 5. The magnified colourmap shows a complex transition described in Section 3.4, with areas of networks with canonical dynamics (green) giving way abruptly to networks with unorthodox dynamics (white) in some dimensions, while changing slowly in other dimensions (here, changing into yellow and red).**
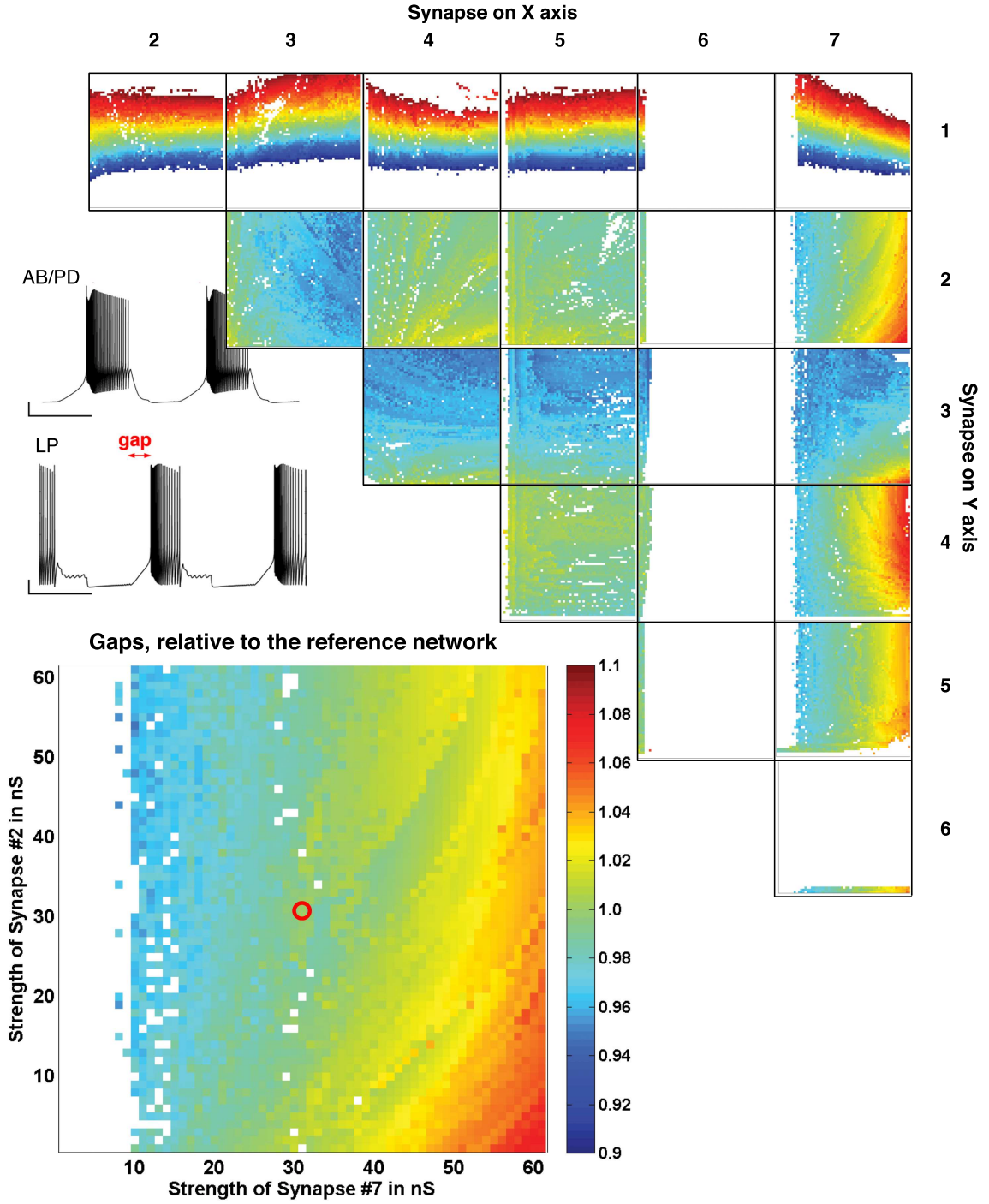
Figure 7: **Colour maps of the ratios of gaps of 78,141 networks to the gap of the reference network (red circle). All colourmaps as in Figure 5. The magnified colourmap shows a transition in two dimensions described in Section 3.4, with areas of networks with larger-than-canonical dynamical metrics (red) giving way smoothly to networks with smaller-than-canonical metrics (blue), while passing through a large band of networks with canonical dynamical metrics (green).**
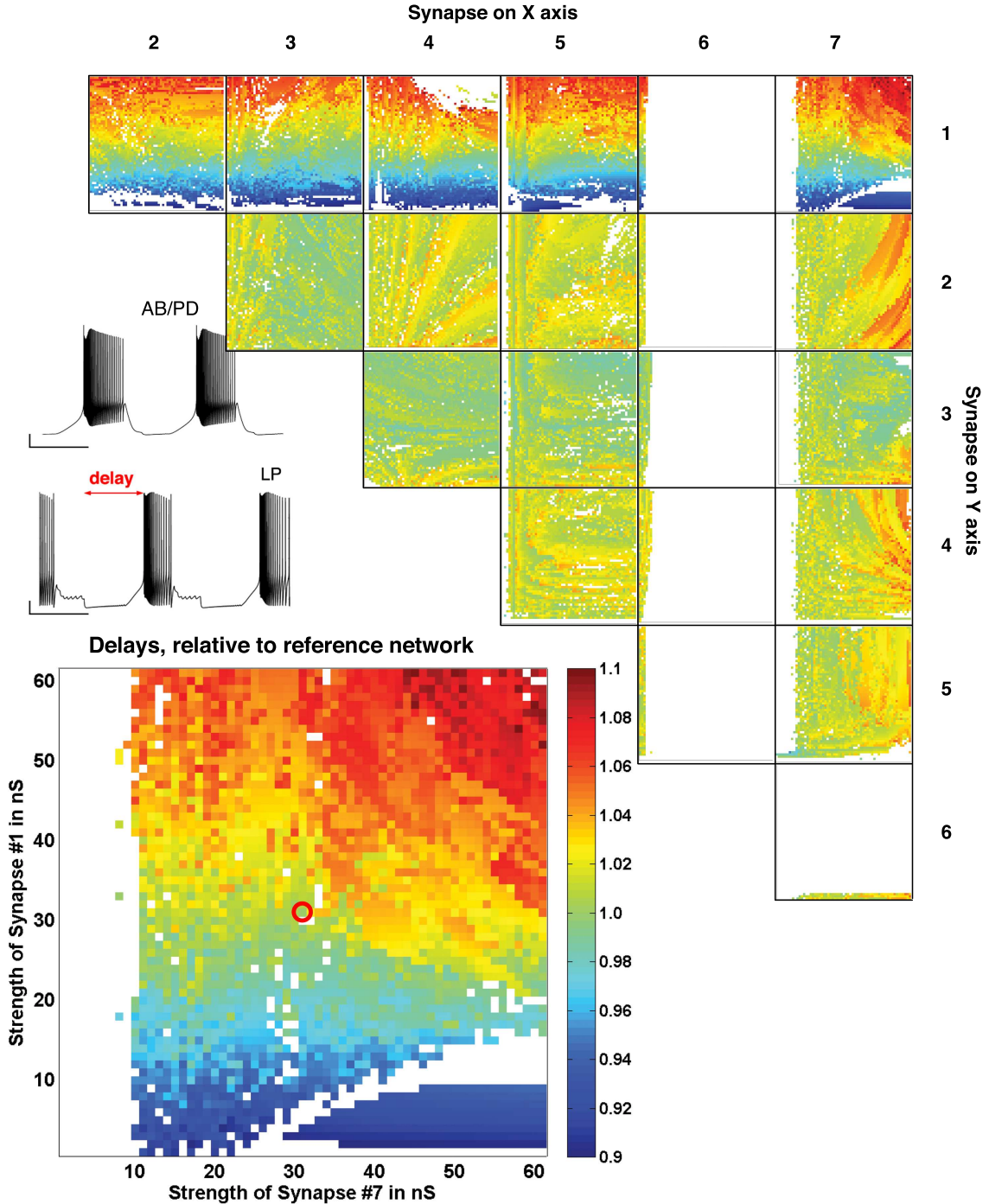
Figure 8: **Colour maps of the ratios of delays of 78,141 networks to the delay of the reference network (red circle). All colourmaps as in Figure 5. The magnified colourmap shows dynamical metrics changing smoothly along Synapse # 1, which connects AB/PD to LP. In contrast, the effect of changing Synapse # 7 is more complex, as Synapse # 7 connects PY to LP, leading to more complex network effects.**
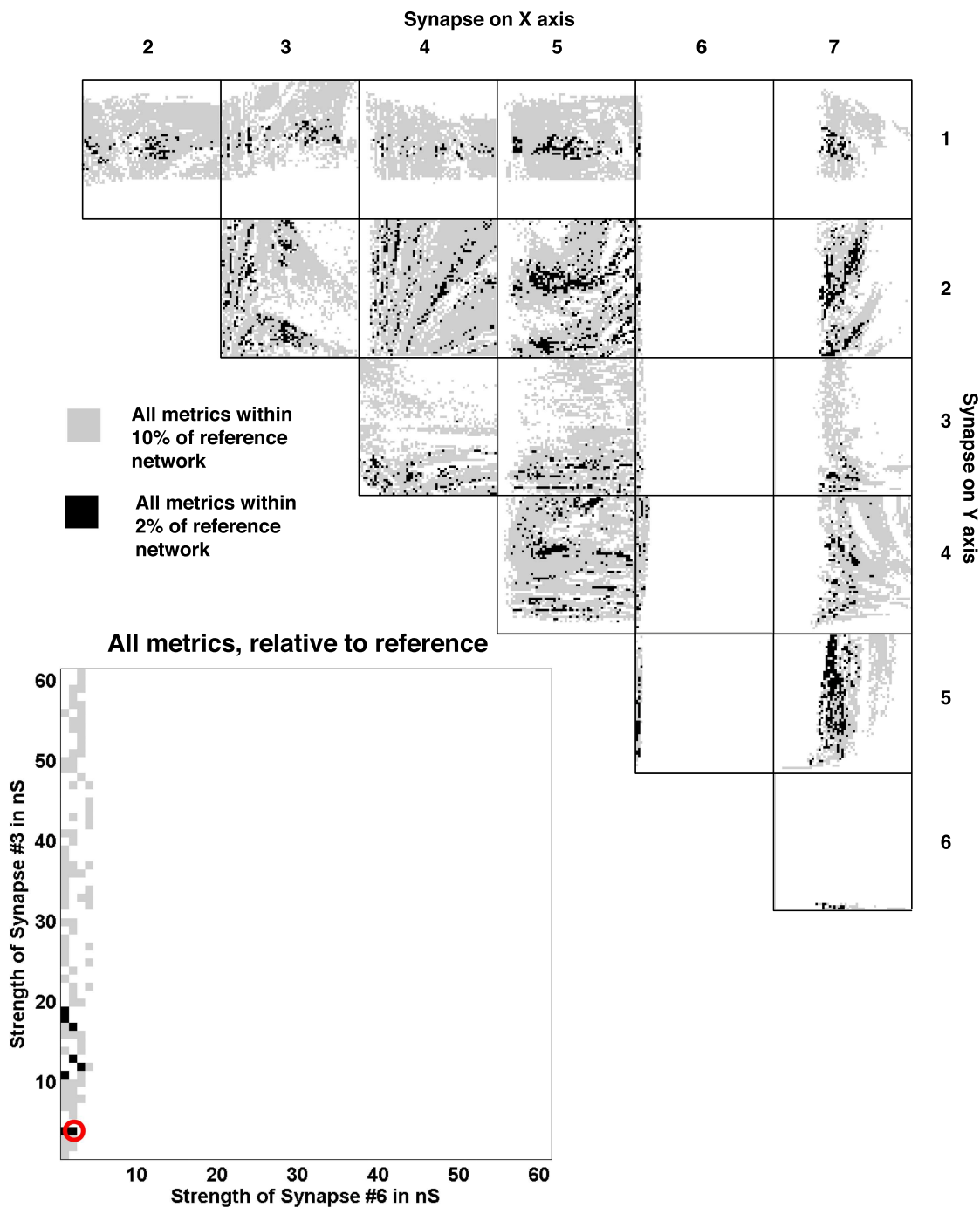
Figure 9: **The ratios of all metrics of 78,141 networks to the ratios of the reference network (red circle). The magnified plot compares the robustness of the two weak synapses, # 6 and # 3. While Synapse # 3 can be increased by an order of magnitude without significantly disrupting the canonical dynamics, the network's dynamics is fragile to changes in Synapse # 6.**

3.3 Pair-wise variation of synaptic strength

I now claim that case (3) is true for the STG network. Furthermore, I assume that the analytical results proved by Memmesheimer and Timme [8, 9] hold in general. The tactics used to substantiate these claims differ from those described above. An analytical approach à la Memmesheimer and Timme is not possible due to the intricate dynamics of the neuron models and of the network. Moreover, performing a parameter search in seven dimensions of a forty-nine-dimensional dynamical system is computationally prohibitive. Furthermore, Prinz et. al. measure the dynamical behaviour of the $\approx 2\text{x}10^7$ networks they simulate against a 'fuzzy' benchmark, i.e., the experimental mean ± 2 s.d. (See Figure 2). In addition, the set of 'pyloric' networks they identify is a union of sets of networks of three distinct origins: sets of networks that show a common behaviour due to topological factors, sets of networks that show a common behaviour due to neuron parameters, and concatenations of the preceding two.

To summarize the results of Prinz et. al. [32], a search over a very broad parameter space for dynamical behaviour with a low-dimensional, tolerant restriction led to the identification of a large number of acceptable solutions.

Working on the assumption that the theory developed by Memmesheimer and Timme [8, 9] apply to networks in general, rather than to some specific analytically accessible examples like LIF networks, I hypothesise that a manifold of at most $n-1=6$ dimensions that lies in the n-dimensional parameter space of the synaptic strengths of the network, exists, and that every network on such a manifold exhibits the same dynamical behaviour. I test for the existence of this manifold by varying synapses in pairs and measuring the dynamical metrics of each network. Thus, for every pair $(s_i, s_j), s \in \{0, ..., 60\text{nS}\}, i, j \in \{1, \ldots, 7\}$, the corresponding network is simulated for 10 seconds, and the the period, duration, gap and delay (see definitions in Figure 3) are computed from the voltage traces in the terminal 5 seconds.[2]

These metrics, computed at each point in parameter space, are compared to the metrics of *one* canonical network. This canonical network was arbitrarily chosen to be network (e) in Figure 3 in [32], which is shown to be 'pyloric'. This canonical network is fully specified by three sets of neuron parameters, and seven synapse strengths, given in [32].

Since the focus of this thesis is to better understand how topology affects dynamics in networks, the neuron parameters are not changed, and remain at the values specified in Table 2 throughout this thesis. Thus, the canonical network is uniquely specified

32

by its seven synaptic strengths: 30, 30, 3, 10, 30, 1, and 30 nS, listed in the order of (arbitrary) synapse labelling in Figure 3. These synaptic strengths are represented by g_s in Equation 6.

To sum up, this approach allows the formulation of a stronger statement on topology-dynamics relationships in the STG network, as all dynamical metrics are measured against *one* chosen network with a *single* characteristic behaviour.

3.4   Simulation Results

Since each synapse was varied from 0nS to 60nS in steps of 1nS, and since there are a total of seven synapses, pair-wise variation requires $21 \times 61 \times 61 = 78{,}141$ simulations. Most networks were 'pyloric', i.e., their triphasic bursting rhythm was within the variation of experimentally observables. The exceptions were networks where the entire rhythm was disrupted, which typically occurred when Synapse #6 was increased.

The normalised metrics of all 78,141 networks are presented in Figure 5 (periods), Figure 6 (duration), Figure 7 (gaps), and Figure 8 (delays). Each figure presents the variation of one metric with all pairs of synapses being varied. For a pair of synapses (i,j), the colour-map in the ith row and the jth column is the representation of $61 \times 61 = 3721$ simulations where this pair of synapses is varied independently from 0 to 60 nS. The metric of interest (e.g. the period in Figure 5) is then coloured according to its ratio to that metric of the reference 'canonical' network. Across all colour-maps in all figures, green is used to represent metrics within 1% of the metrics of the canonical network. Red regions correspond to networks whose metric is larger, but within 10% of the canonical metric, and blue areas correspond to networks whose metric is smaller, but within 10% of the canonical metric. White areas denote networks that either do not have a meaningful metric, due to a failure to display a pyloric dynamical state, or whose metric is more than 10% away from that of the canonical network.

Figure 9 presents concatenations of all metrics for all 78,141 networks. Networks shown in Figure 9 are those with all four metrics within either 2% (black) or 10% (gray) of the reference network.

---

[2]The metrics are computed from the terminal half of the simulation to avoid transient artefacts.

3.4.1   Patterns in Parameter Space

The main result of these simulations is that a large number of networks with behaviour very close to that of the canonical network exist, and that these networks are *not* randomly distributed on the parameter planes. Instead, networks with similar dynamics are found in basins, lines, regions and points in the parameter planes.

This underscores the idea that the dynamics of the network is robust to changes in some synapses (as shown in the lines and regions in some dimensions) but fragile to changes in other synapses (as shown by the lines: moving perpendicular to the lines rapidly destroys the observed dynamical state). An illustrative example of the latter is the critical dependence on Synapse #6. Much of the parameter plane where one of the axes is Synapse #6 is white, meaning that the network doesn't exhibit the characteristic triphasic burst of the STG network. In other words, significant variations Synapse #6 completely destroy the pyloric nature of the output. This is in excellent agreement with earlier results from Prinz et. al.'s more coarse-grained parameter search, and from experiments [32].

However, Synapse #6 is critical only on *increasing* its strength. In a more subtle prediction not stated by [32], it can be seen (Figure 9, magnified plot) that in most cases, Synapse #6 can be removed, preserving the functional output of the circuit almost undisturbed. The functional and evolutionary consequences of a synapse that is not essential, but whose strength cannot exceed an upper threshold, could be a matter of considerable interest.

Clear and well-formed patterns in parameter space of networks that exhibit near-identical dynamics (green dots in Figures 5,6,7 and 8) are seen for all metrics. This is strong evidence in support of the claim that all networks that exhibit the same dynamical state lie on a high-dimensional manifold in parameter space. Apart from networks whose dynamical states are close to that of the canonical network (green, in every figure), it is interesting to note that there are several other patterns of networks exhibiting a different, common dynamical state. Bands of networks with higher, uniform gaps can be seen coloured red in Figure 7. Large regions and lines of parameter space contain networks with a shorter period, seen coloured dark blue in Figure 5. This isn't surprising: there's nothing special about the dynamical state of the canonical network. Just as there is a manifold in parameter space containing networks whose dynamics map onto the dynamics of the canonical network, so are there *other* manifolds, containing networks whose dynamical states correspond to some other, unknown, common

reference.

3.4.2 Transitions in Parameter Space

Transitions of the dynamical behaviour of the network, from unorthodox (white) to larger than canonical (red) to canonical (green) to smaller than canonical (blue) back to unorthodox (white) are observed in these parameter planes. These transitions are of some specific types:

1. **Smooth transitions in one dimension:** Dynamical metrics change smoothly and almost monotonically in one dimension (one synaptic strength), while the effect of changing the other synaptic strength is minimal. This can be seen in Figure 7. Here, the gap metric changes smoothly along Synapse#1, and is insensitive to all other dimensions (except Synapse#6).

2. **Smooth transitions in two dimensions:** Dynamical metrics change smoothly and almost monotonically in a direction not parallel to the synaptic axes. This can be best seen in the colour map of gaps (magnified in Figure 7) with Synapse#2 and #7 being varied.

3. **Sharp cutoffs:** Dynamical states change sharply from canonical to unorthodox. The sharpness of this transition exceeds the resolution of the simulation (1 nS). Every parameter plane involving Synapse #6 shows this: below the critical limit of Synapse #6, dynamical states are characterized by near-canonical metrics. Above this limit, the entire pyloric rhythm breaks down. (Figures 5,6,7 and 8)

4. **Complex accordion transitions:** Multiple, often bent bands of canonical networks, interleaved with bands of higher or lower metrics, are seen in the parameter plane. Examples of this can be seen in the periods of Synapse#4 (Figure 5). This may indicate that the manifold 'ripples' in higher-dimensional parameter space, as a two-dimensional section through a ripple would show interleaved bands of canonical and unorthodox networks, like an accordion.

5. **Higher-order transitions:** More complex transitions, as seen in the durations, varying Synapse #3 and #2. This may indicate oblique intersections of the manifold with the parameter plane. Since only two parameters are varied in each experiment, the true structure of the manifold cannot be precisely determined.

However, the presence of these transitions indicates the high-dimensional nature of the manifold. This is shown magnified in Figure 6.

What do these transitions mean? Firstly, their presence, especially that of the higher-order transitions and complex accordion transitions, is additional evidence for the existence of a manifold on which all dynamically identical networks lie.

Smooth transitions in two dimensions suggest that one synapse can compensate for another, not necessarily in a linear manner. If the lobster STG network has mechanisms that regulate such a transition, the network is substantially robust to changes in synaptic conductances, caused, say, by injury.

The existence of complex accordion transitions suggests some intriguing behaviour. If the strength of Synapse#4 is 'tuned' from 60nS to 0nS, (imagine moving on a line parallel to the abscissa in the magnified plot in Figure 5) the target canonical dynamics disappears initially, then reappears on decreasing the strength further, then disappears again, and so on. If one were unaware of this transition, this behaviour would appear perplexing.

4 From Dynamics to Topology

"As coupled oscillators, women are far subtler than fireflies" — Steven Strogatz [50]

To close the loop between network structure and dynamics, methods to predict the structure of a network, given its dynamical behaviour, need to be developed. In this section, a few chosen methods to reconstruct networks (genetic, neuronal and sociological) are briefly presented. In Sections 4.2.1 and 4.2.2, a method described by Timme in [28, 11] will be introduced and refined, and demonstrated to reconstruct the effective coupling strengths of a network of Kuramoto oscillators.

4.1 Network Reconstruction: An Overview

Network reconstruction is a topic of interest to systems biologists seeking to understand the interplay of the complex network of genes, metabolites and proteins in a cell. Kim et. al. [20] model the dynamics of gene networks using a system of coupled differential equations, and propose a method to infer the structure of the network from time-series of gene expression. They demonstrate this technique to reconstruct the gene network in the budding yeast cell cycle, and show that, at least in synthetic gene expression data, the method works even in the presence of noise and delays.

While this technique is passive, requiring only a set of time series from the system, 'active' methods based on perturbation theory have also been developed. Gardner et. al. [21] induce transcriptional perturbations to the relaxation dynamics of gene concentrations to their fixed point to reconstruct a nine-gene sub-network in *Escherichia coli*. A similar approach is used by Dharmadi et. al. [12], with the development of a modelling tool they call Elementary Network Reconstruction (ENR). By ignoring the dynamics of gene expression levels, and by focusing on their steady-state solutions,

Dharmadi et. al. reconstruct the gene interaction network by inducing perturbations to the steady state gene expression levels, and use Taylor series expansions around the unperturbed state to build models of the perturbations.

Tegner et. al. [29] underscore the importance of micro-array technology in reconstructing large gene networks. The demonstrate that the perturbation of a few key genes is sufficient to reveal the structure of the gene network. Their approach, like that of Dharmadi et. al. [12] and Gardner et. al. [21], focuses on the steady state values of gene expression levels, as the determination of transient dynamics in gene expression is still a technical challenge. To summarise, the four methods sketched here attempt to reconstruct genetic networks either by using information theoretic measures, like Kim. et. al., or via linear perturbation theory, as in Dharmadi et. al. [12], Garnder et. al. [21], or Tegner et. al. [29].

It is important to state that methods of network reconstruction are constrained by the limitations of access to the network at hand. Thus, while some methods may work for some systems, others are more suitable for systems differing in experimental accessibility, size or dynamical complexity.

While multi-unit recording systems like flat multi-electrode arrays provide access to many dimensions of a cultured neuronal population, deciphering its structural and functional connectivity is a non-trivial matter. Makarov et. al. [3] present a method to create a model of a neuronal network using extracellular spike recordings. Their approach is straightforward: they create a deterministic model of a spiking neuronal network, and tune the model's parameters by stochastic optimisation till the dynamic behaviour of the model fits experimental data well. Using this approach, they are able to predict, to some degree of approximation, spikes in the future from the real neuronal network.

Kramer et. al. [23] study the uncertainty of edge likelihood in reconstructed networks, where edges in their reconstructed network are generated by functional connectivity in a multivariate time series exceeding some predetermined threshold. Since there is uncertainty in the measurements of a network induced by the limitations of experimental design, they suggest that it is important to include a measure of this uncertainty into the models of networks that are reconstructed. Thus, the output of their procedure consists of both the reconstructed network and a quantification of uncertainty of the number of edges. They apply this technique to electrocorticogram data from a human during an epileptic seizure.

Another approach to quantify the uncertainty in network reconstruction is presented

by Guimera et. al. [22]. Without assuming complete reliability of available network data, they present a mathematical framework to reliably identify both missing and spurious interactions in noisy and unreliable observations of network dynamics. They further show that their approach is powerful enough to reconstruct networks from noisy observations that are closer to the 'true' network than the noisy observations themselves.

This overview of network reconstruction will conclude with two abstract methods to reconstruct networks of coupled oscillators, modelled by the Kuramoto system. Arenas et. al. [33] demonstrate a method to reconstruct the community structure of a network by measuring how fast sub-graphs within the network synchronise. The idea is that densely connected communities in a larger network synchronise first. They show that well-defined modular structures, characterised by distinct topological scales, emerge at different time scales, allowing for a partitioning of the graph into communities. However, they stop there, and do not attempt to reconstruct the entire network based on speeds of synchronisation.[3]

Zanette [27] introduces a method to reconstruct a network of Kuramoto oscillators in the fully synchronous state by inducing an external perturbation to one node. By showing that the response of each oscillator is well-defined function of its distance from the perturbation, Zanette suggests that the network may be reconstructed by inducing a set of perturbations on different nodes in the network.

4.2   Reconstructing networks...

The focus of this section will be based on a method for network reconstruction first described by Timme [28, 11]. It is detailed and refined for the Kuramoto system, and it is hoped that that it can be used to reconstruct the network for the lobster STG.

This network reconstruction method assumes that the network is composed of a system of oscillators as in the Kuramoto Model, and that the network settles into a phase-locked attractor that is at least stable to small perturbations. In contrast to Zanette's method, a fully synchronous state of the network is not required. The assumption of a phase-locked attractor is hoped to be reasonable for the STG model, as in the functional STG system, each neuron acts as an oscillator, and the pyloric

---

[3]Preliminary studies show that it may be possible to reconstruct an undirected network simply by measuring the speeds of synchronisation between nodes. Naturally, this technique only works with a initial conditions close to the synchronous attractor.

rhythm is defined by characteristic phase differences between the neurons. However, before attempts are made to reconstruct the real pyloric net, the reconstruction was tested on the a simpler mimic, with the Kuramoto model running on a graph with equivalent edge weights.

4.2.1   ...with N experiments

Timme [11] described a method to reconstruct the effective coupling constants of a N-node network by performing at most N experiments, where all the neurons are driven by an arbitrarily chosen current vector $\bar{I}_m$ for the mth experiment. Thus, the current to the ith neuron in the mth experiment is $I_{i,m}$. Thus the dynamics of the ith neuron is given by

$$\dot{\phi}_i = \omega_0 + \sum_{j=1}^{N} J_{ij} f(\phi_i - \phi_j) + I_{i,m} \tag{10}$$

For the undriven condition, $\bar{I}_m = 0$, and the system settles into a phase-locked cycle characterised by a collective frequency Ω_0 and N-1 independent phase offsets

$$\Delta_{ji,0} = \phi_{j,0} - \phi_{i,0} \tag{11}$$

which is time-invariant. The driven system is equivalently characterised by a collective frequency

$$\Omega_m = \omega_0 + \sum_{j=1}^{N} J_{ij} f(\phi_i - \phi_j) + I_{i,m} \tag{12}$$

and phase offsets $\Delta_{ij,m} = \phi_{j,m} - \phi_{i,m}$. If the driving currents are sufficiently small, then the perturbed phase locked cycle is close to the original limit cycle:

$$|(\phi_{i,m} - \phi_{j,m}) - (\phi_{j,0} - \phi_{i,0})| \ll 1 \tag{13}$$

Taking the differences for the phase-locked conditions for the driven and undriven systems, we get

$$D_{i,m} = \sum_{j=1}^{N} J_{ij} f(\phi_{i,m} - \phi_{j,m}) - f(\phi_{j,0} - \phi_{i,0}) \tag{14}$$

where $D_{i,m} = \Omega_m - \Omega_0 - I_{i,m}$. For sufficiently small perturbations, equation (13)

holds, and we approximate $f(\phi_{i,m} - \phi_{j,m}) = f(\phi_{i,0} - \phi_{j,0}) + f'(\phi_{i,0} - \phi_{j,0})(\Delta_{ij,m} - \Delta_{ij,0})$. Thus, equation (14) can be rewritten as

$$D_{i,m} = \sum_{j=1}^{N} \hat{J}_{ij}\theta_{j,m} \tag{15}$$

where $\theta_{j,m} \equiv \phi_{j,m} - \phi_{j,0}$ and $\hat{J}_{ij}$ is a Laplacian matrix given by

$$\hat{J}_{ij} = \begin{cases} J_{ij}f'(\Delta_{ij,0}) & i \neq j \\ -\sum_{k,k\neq i} J_{ik}f'(\Delta_{ki,0}) & i = j \end{cases} \tag{16}$$

For each experiment, *N-1* independent phase offsets and one collective frequency Ω_m are obtained, yielding N linear equations that restrict the N^2-dimensional space of possible network topologies. Thus, after performing *M=N* experiments, the space of networks is restricted to exactly one, and the effective coupling strengths can be deduced by

$$\hat{J}_{ij} = D\Theta^{-1} \tag{17}$$

where Θ is the $N \times N$ matrix of all θ.

As demonstrated earlier [28], even large networks can be efficiently and accurately reconstructed. However, for *N=3*, and the connection strengths proportional to synaptic conductances of the STG network, this method failed. Specifically, it did not succeed in identifying the 'synapse' that was absent, and failed to estimate the absolute strengths of the individual synapses. This problem was traced to the fact that the matrix $\hat{J}$ generated by the algorithm was no longer Laplacian. Nothing in Equation (17) specifies the Laplacian constraint on $\hat{J}$.[4]

To circumvent this, I exploited a further degree of freedom in θ, the matrix of phase offsets. Adding a constant to a row in θ changes θ, as it is a different matrix. However, this operation still represents the same physical system.

Based on this idea, I scanned the *N*-dimensional space of phase offsets for a θ that yielded a set of solution matrices $\hat{J}_{ij}$ that is as close, in Euclidean norm, to the Laplacian as required. The 'correct' solution was identified among this solution set by picking the solution that corresponded to the smallest differences among D.

While this is an *ad-hoc* numerical recipe to reconstruct small networks, it is awk-

---

[4]Interestingly, this problem becomes less relevant with increasing N. With N=32, a fairly good reconstruction was achieved because most of the matrices returned *were* Laplacian.
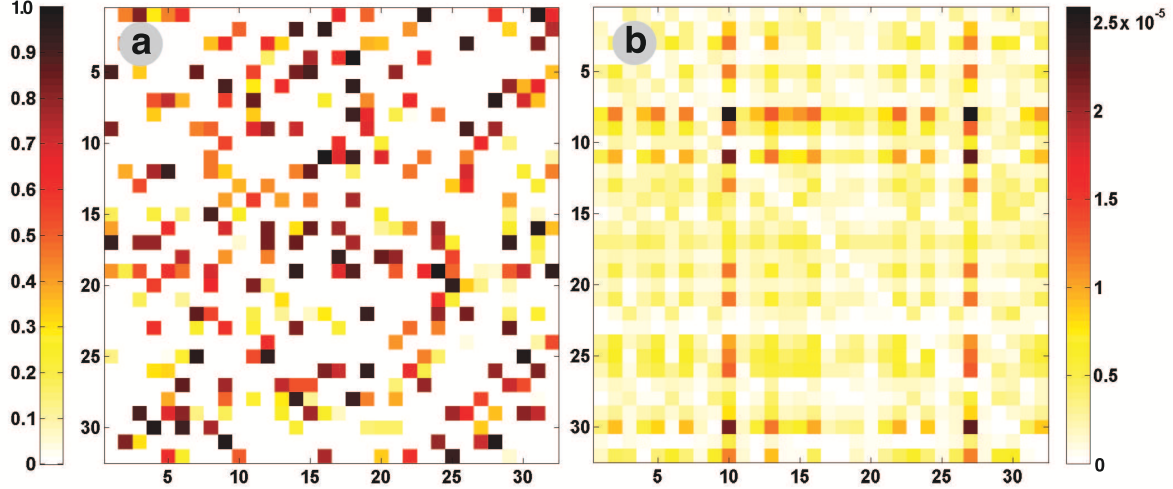
Figure 10: **Reconstructing a 32-neuron network of Kuramoto oscillators. (a) Colourmap of the reconstructed connectivity matrix of the network. (b) Absolute differences between reconstructed and actual network. Note the magnified scale. The reconstruction is carried out according to Section 4.2.2.**

ward and mathematically unsound. In addition, it isn't clear if multiple solutions are permitted, or even possible.

4.2.2   ...with N-1 experiments

To clear away these ambiguities, the theory is reformulated as follows.

For the undriven system, the dynamics of the phase variable are given as before by

$$\dot{\phi}_i = \omega_0 + \sum_{j=1}^{N} J_{ij} f(\phi_i - \phi_j) \tag{18}$$

This system settles asymptotically into a phase locked attractor, characterised by *N-1* independent phase offsets and a single collective frequency Ω_0. Without loss of generality, we measure these phase offsets w.r.t the first neuron:

$$\Delta_{j,m} = \phi_{j,m} - \phi_{1,m} \tag{19}$$

for $m\epsilon\{0, 1, \ldots, N-1\}$ and $j\epsilon\{1, 2, \ldots, N\}$. Now, when the system is driven with some current vector $\bar{I}_m$, the asymptotic dynamics of the phase variable follow

$$\dot{\phi}_{i,m} = \omega_0 + \sum_{j=1}^{N} J_{ij} f(\phi_{i,m} - \phi_{j,m}) + I_{i,m}$$

$$= \omega_0 + \sum_{j=1}^{N} J_{ij} f(\Delta_{i,m} - \Delta_{j,m}) + I_{i,m}$$

$$= \omega_0 + \sum_{j=1}^{N} J_{ij} \left[f(\Delta_{i,0} - \Delta_{j,0}) + f'(\Delta_{i,0} - \Delta_{j,0})((\Delta_{i,m} - \Delta_{j,m}) - (\Delta_{i,0} - \Delta_{j,0})) \right] + I_{i,m}$$

$$= \Omega_0 + \sum_{j=1}^{N} \hat{J}_{ij}((\Delta_{i,m} - \Delta_{j,m}) - (\Delta_{i,0} - \Delta_{j,0})) + I_{i,m} \tag{20}$$

where elements in $\hat{J}$ are products of the coupling strength and the derivative of the coupling function evaluated at the asymptotic phase difference.

$$\hat{J}_{ij} = J_{ij} f' (\Delta_{i,0} - \Delta_{j,0}) \tag{21}$$

On performing *N-1* experiments, all *N(N-1)* off-diagonal elements of $\hat{J}$ can be computed from

$$\Lambda = \bar{J} P \tag{22}$$

where Λ is a *N* by *N-1* matrix containing the frequency components

$$\Lambda_{i,j} = \Omega_m - \Omega_0 - I_{i,m} \tag{23}$$

and *P* is a square matrix of size *N-1* containing the phases offsets $\delta_{ij,m} = (\Delta_{i,m} - \Delta_{j,m}) - (\Delta_{i,0} - \Delta_{j,0})$ and $\bar{J}$ is a *N* by *N-1* matrix of off-diagonal terms of *J* specified by

$$\bar{J} = \begin{bmatrix} J_{12} f'(\Delta_{1,0} - \Delta_{2,0}) & ... & J_{1N} f'(\Delta_{1,0} - \Delta_{N,0}) \\ -\sum J_{2j} f'(...) & J_{21} f'(...) & ... \\ J_{31} f'(...) & ... & ... \\ ... & ... & -\sum J_{Nj} f'(...) \end{bmatrix} \tag{24}$$

$\bar{J}$ is merely a reordering of the off-diagonals of $\hat{J}$ to explicitly specify the Laplacian restriction on $\hat{J}$. Thus all off-diagonal elements of the network are reconstructed with *N-1* experiments. This can be understood intuitively by the fact that an *N*-node network

that settles into a phase locked state is formally an *N-1* dimensional system, as the interaction terms can be rewritten in terms of the *N-1* independent phase differences.

How does this remove the ambiguities in the earlier formalism? The crux of the matter is in the explicit reformulation of $\hat{J}$ as a *N* by *N-1* dimensional matrix, which removes the diagonal (self-coupling) terms of the adjacency matrix. This analytical constraint is the *exact* version of the numerical trick described in Section 4.2.1.

For the Kuramoto system with weak positive couplings, sine interaction functions and uniform intrinsic frequencies, the attractor of the undriven system of a generic network is the fully synchronous state. Thus the pre-factors $f'(\Delta_{i,m} - \Delta_{j,m})$ are simply 1. This means that the matrix of reconstructed effective coupling strengths is very close to the matrix of actual coupling strengths *J*, leading to a good reconstruction of the network.

A reconstruction based on this theory is shown in Figure 10. Panel (a) shows the reconstructed 32-neuron network, and panel (b) shows the differences between the reconstructed network and the real network.

4.2.3   Reconstructing Inhibitory Networks

However, for inhibitory networks, the synchronous state is no longer stable. Specifically, for a three-neuron network with global, uniform, negative coupling, the attractor is characterised by $|\Delta_{1,0}| = |\Delta_{2,0}| = 2\pi/3$. This means that (1) the pre-factors are no longer necessarily close to 1, and (2) the strength of the pre-factor may obscure the strength of the coupling constant. In the most extreme case, $\hat{J}_{ij} = 0$ because $f'(\Delta_{i,0} - \Delta_{j,0}) = 0$, thus preventing any estimation of J_{ij}.

Thus, even when the coupling function is known, as in the Kuramoto Model, it is not possible to predict the network's *structural* connectivity, though the network's *functional* connectivity can be revealed as before. Structurally, the only prediction possible is the absence of a synapse, but even that cannot guarantee an absence of false positives.

Some subtle differences in inhibitory networks are worth mentioning. While the standard Kuramoto system with positive couplings and uniform frequencies eventually synchronises and oscillates with a collective frequency given by ω_0, the inhibitory Kuramoto system, apart from failing to synchronise, settles into a collective phase locked state whose frequency typically differs form ω_0. This is because a failure to synchronise implies a set of phase differences between the neurons that are not all zero. The effect

of f on these phase differences is typically non-trivial, leading to a collective frequency different from ω_0.
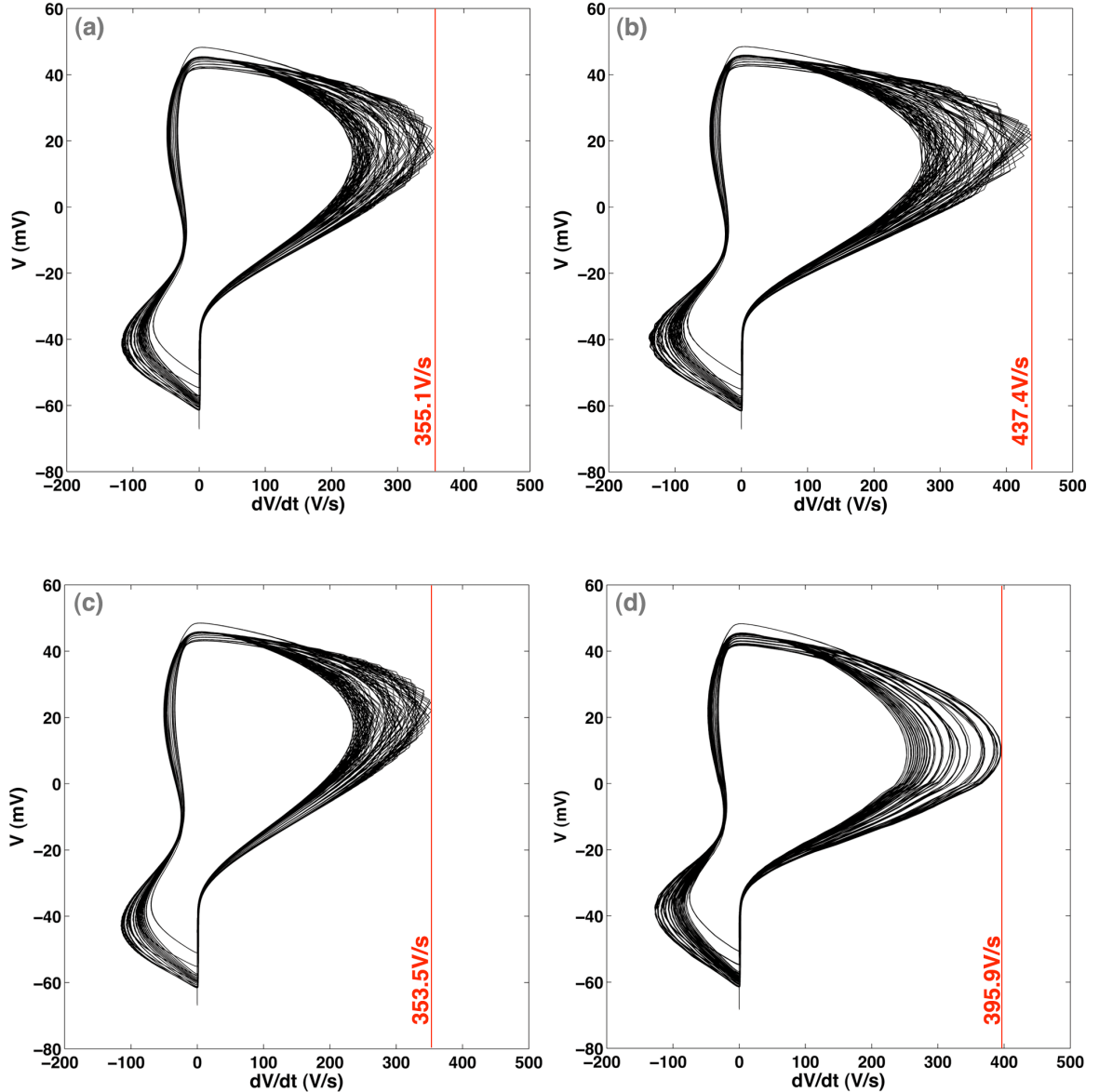
Figure 11: **Phase Portraits of four Simulations of Neuron AB/PD # 3, displaying aperiodicity of this neuron model. (a) Using the exponential method described in Dayan and Abbott [36] (b) Using the Hybrid method described in Prinz et. al. [35] (c) Output from the Simulator provided by Prinz et. al. [5] (d) Using the ode23t solver in MATLAB. All phase portraits are for 10 seconds. (a) and (b) use a step size of 50 μ s.**

45

4.3   Reconstructing the STG network

The primary purpose for introducing the network of Kuramoto oscillators was to develop a simplified model of the STG network on which methods to reconstruct networks could be tested. As detailed in Section 4.2.2, this method can reconstruct the effective coupling strengths of a network of *N* oscillators in *N-1* experiments.

However, attempts to reconstruct the STG network based on these methods failed. This was due to the fact that the STG network, and the neurons in isolation, exhibited aperiodic dynamics. Evidence for the aperiodicity of a single neuron is presented in Figure 11. Phase portraits of four simulations of Neuron AB/PD #3, using different numerical methods, show that trajectories form a dense band, and do not superimpose, showing that, at least for the best numerical methods available, the neuron does not show periodic behaviour.

The methods described in Section 4.2.2 require the periodicity of individual neurons and the periodicity of the network. The STG network fails to achieve either. A more detailed discussion of the aperiodicity of the neuron model, is given in Section 6.2.

5   Conclusion

"Any sufficiently advanced technology is indistinguishable from magic."
—Arthur C Clarke

The study of networks is still in that embryonic stage where much of the function and effects of networks amaze, rather than illuminate. However, like the evolution of all sciences, amazement leads to questions, and with the slow but inevitable answering of questions, awe gives way to comprehension. Stanley Milgram's famous experiment demonstrating 'six degrees of separation' between any two people in the world [52, 51] brought the concept of 'small worlds' to a scientific and lay audience, and prepared the stage for founding a theory of small-world topology [53]. Network structures first observed in sociology were rediscovered in the brain [55, 54].

The study of networks is important in several crucial ways. From formulating theories of social dynamics and economic theories based on experimentally testable models, to understanding brain dynamics, network science is at the forefront of many fields of research. The Singularity, the point in human history when the creation of a self-replicating exponentially growing autonomous intelligent system is possible [56, 57], may not be reached without a deep understanding of how our brains work [58].

That said, this thesis presents a small understanding of the core interrelations between network structure and dynamics. I have shown that principles governing the relationship between network topology and dynamics, proved for simpler systems, hold even for the biophysically-detailed model of the STG network of the lobster. Given previous theoretical results [8, 9] and the work presented here, it seems likely that most networks, irrespective of topological constraints or node dynamics, obey similar rules.

The consequences of the results presented in Section 3.4 are intriguing in a biological setting. Given the existence of this manifold of dynamically-identical networks, it is clear that regulatory systems on the network have a variety of mechanisms by which behavioural output of the STG can be controlled. The large extents of these manifolds

underscore the robustness of the STG network to random perturbations of structure. At the same time, the fragility of the dynamical output to increases in strength of Synapse#6 may suggest the existence of a 'switch', where the varying of a single parameter — the strength of Synapse#6— by a small amount can switch the network between functional and nonfunctional states.

Some questions linger: is the sharp cutoff seen on increasing Synapse#6 a true phase transition, or is the transition steep but smooth? Sampling of the parameter plane at a higher resolution may resolve this. While this thesis has described how some differently-structured networks might behave, the question of how the network might evolve has been neglected. Specifically, how do the neurons make initial connections and self-organise to a functional network? How do the manifolds control the trajectory of the evolving network through parameter space? Could a random walk through parameter space efficiently find a point on the manifold corresponding to the target dynamics?

Further, I have demonstrated and refined a technique to reconstruct networks, making only minimal assumptions on its structure. Since this technique perturbs the network's dynamical system from its limit cycle, a functional understanding of its structure can be obtained. For systems like the a network of Kuramoto oscillators, this method can reveal the functional connectivity of the network.

Given recent advances in optical imaging techniques and optogenetic means of perturbing a neuron, it may be possible to reconstruct the effective coupling strengths of a network of oscillatory neurons that are otherwise inaccessible. Such an experimental technique would provide direct methods to study real, neuronal networks in functioning states. A first step would be to test the reconstruction methods described here on a simpler model of the STG, for example, one based on the Hindmarsh-Rose bursting neuron model [38].

Of Steven Strogatz's list of complexities [41] that networks can exhibit, (in Section 1.1 of this thesis), theories in Network Science typically ignore most of them, to focus on one type of complexity. For example, the theory of reconstruction of networks presented in Section 4.2.2 uses the Kuramoto Model, thus circumventing additional layers of complexity: network evolution, connection diversity, dynamical complexity and node diversity, to focus solely on the structural complexity of the network. While such approaches provide good lines of attack to the problems in Network Science, the ultimate goal is to develop theories powerful enough to deal with all these types of complexities.

6 Appendix

6.1 A Note on Neuron Models

Over the course of the development of the STG model, Prinz et. al., the authors of [35, 32, 5] have used different approaches to solving the differential equations governing the dynamics of the STG neuron. In their first paper on the subject, they use Euler's method, presumably of first order, with a time step of 25 μs [35]. In another paper published later that year [5], they introduce and implement the hybrid method, where the gating variables are integrated with Euler's method (with a time step of 50 μs) and the voltage and Calcium concentration are integrated using the exponential method of Dayan and Abbott [36].In their latest paper on the subject [32], they state they used the exponential Euler method, presumably using this method to integrate all dynamical variables.

However, they do not use more sophisticated methods like the 4/5-Runge-Kutta method or methods developed for solving 'stiff' equations like the Shampine-Reichelt-Kierzenka trapezoidal rule using free interpolants [39]. It was observed that explicit methods (like exponential Euler, hybrid or Euler) ran up to 100 times faster that implementations of the ode45 or ode23t ODE solvers (which correspond to the Runge-Kutta 4,5 and Shampine-Reichelt-Kierzenka methods) in MATLAB. In simulating a very large number of networks, speed may be more crucial factor than precision.

A comparison of all the methods listed above in simulating neuron LP#4 (whose parameters are specified in Table 2, adapted from [32]) sheds light on both the performance of these methods and the methods apparently used by Prinz et. al.

The benchmark for precision is the Shampine-Reichelt-Kierzenka method [39], implemented in the ode23t solver in the MATLAB framework. Runge-Kutta methods, especially the 4th-order Runge-Kutta method fail due to the 'stiff' nature of the prob-
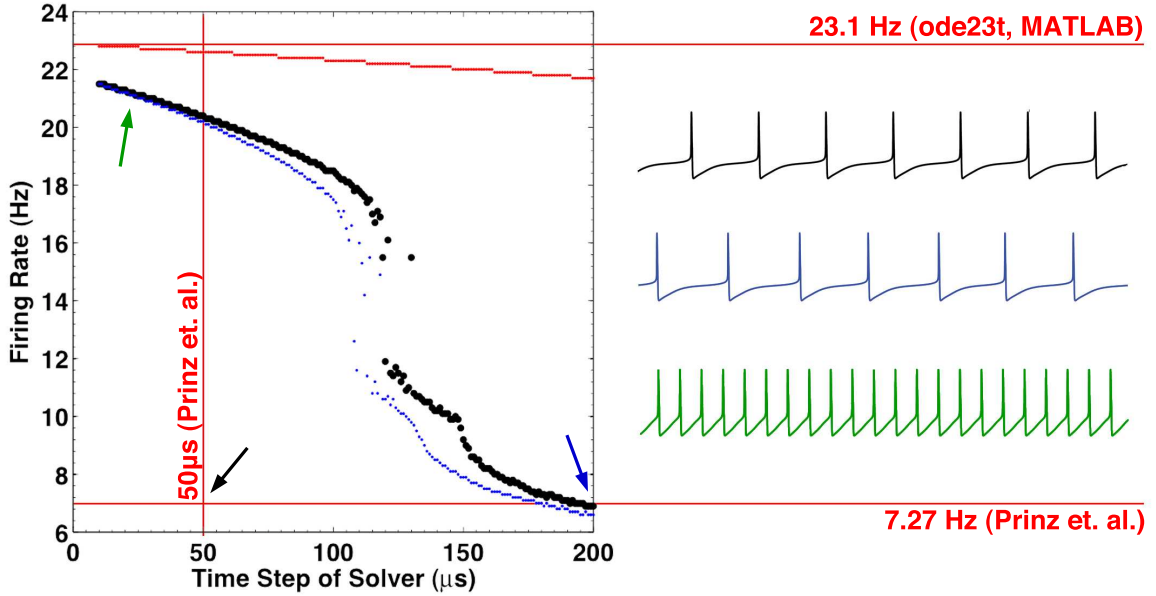
Figure 12: **Numerical Instabilities and precision of solvers for neuron LP # 4 (parameters specified in [32], model described in Section 2). The plot on the left shows the firing rate reported by different solvers at varying time steps. The time step axis does not apply to the ode23t solver, or to the simulation from Prinz et. al. [5]. The plots are: exponential Euler (red dots), hybrid method (black dots), first-order-Euler (blue dots). On the right are three voltage traces for LP # 4 for one second, plotted on the same scale. The black trace is the output from Prinz et. al.'s simulation [5]. Green and blue are from the Hybrid solver. The coloured arrows indicate the positions of the three traces in the plot.**

lem. Figure 12 shows a comparison of the performance of ode23t, exponential Euler (red dots), hybrid (black dots), and Euler methods (blue dots) to a simulation from Prinz et. al. [5]. The temporal step sizes of ode23t and the Prinz et. al. simulation can't be varied, the former by design and the latter due to the non-disclosure of source code. For all other methods, the step sizes are varied from 10μs to 200μs.

First, the robust nature of the exponential Euler method is clear. Even at very large step sizes, the exponential Euler method (red dots) varies minimally from the solution at much higher temporal resolutions. Furthermore, the exponential Euler method approaches the 'real' solution, hereby assumed to be given by the Shampine-Reichelt-Kierzenka method (ode23t).

Secondly, it is startlingly clear that while *all* methods — even the Euler — approach a firing rate between 22-23Hz, the simulation from Prinz et. al. is much lower, at 7.27Hz. The convergence of *four* different methods strongly suggests that the 'true' firing rate of neuron LP#4 is $\approx$23Hz.

50

This leads to puzzling questions about the implementation of the methods used by Prinz. et. al. in [32, 5, 35].

The firing rate suggested by the exponential Euler method is over three times the firing rate reported by Prinz et. al., over a very broad range of solver time steps. Both the Hybrid method and the Euler method, at a time step of 50μs, fail to report the firing rate of LP#4 as even close to 7.27Hz, the frequency reported by Prinz et. al.'s simulation application.

More worryingly, there is reason to believe that this unknown, irreproducible method was used in their paper involving $2\text{x}10^7$ network simulations [32], leading to irreproducible behaviour in the networks they report. The first network (a) in Figure 3 in [32] clearly shows LP#4 firing at approximately 7Hz. Since AB/PD and PY are silent in this network, a simulation of this network is equivalent to the simulation just LP#4, for LP#4. The authors of this paper state that they used the exponential Euler method to simulate these networks [32]. This is in contradiction to the results presented here, where LP#4, solved with the exponential Euler method, never dropped below 20Hz, even at very large time steps.

Without access to the source code behind their simulation application (which is a Microsoft Windows-only executable), the only conclusion that can be drawn from the irreproducability of Prinz et. al.'s simulation is that there is a contradiction between the method and time step presumably used and the output of their simulation application.

6.2 Aperiodicity of Neuron models

The main reason attempts to reconstruct the STG network from their phase responses failed was due to fact that the network is not strictly periodic.

Some elaboration is needed here. The STG network *is* periodic in the sense that inter-burst intervals have a well-defined mean, as do various other metrics. However, it is *not* periodic in the dynamical systems sense of the term. A system S with dynamical variables $(s_1, s_2, \ldots, s_n)$ is periodic and has a period T if, for all t and i,

$$s_i\left(t + T\right) = s_i\left(t\right) \tag{25}$$

In this sense, neither the network nor individual neurons exhibit periodic behaviour. This variation from periodicity is not uncommon in high-dimensional systems. Figure 11 shows phase portraits of a single variable, the voltage, of the spontaneously burst-

ing neuron AB/PD #3, illustrating this aperiodicity. The large voltage excursions correspond to action potentials, and the inter-burst evolution is captured in the nearly vertical parts of the trajectory. In a single 'period', the neuron circles the origin n times, where n is the number of spikes fired every burst.

Two things stand out in the phase portraits. First, the aperiodicity of the neuron is evident in the dense tangle of trajectories. If the neuron was periodic, trajectories of individual spikes would superimpose. Secondly, it is clear that all the explicit methods (exponential Euler, Hybrid, and the simulation from Prinz et. al.) show artefacts in the upstroke of the action potential, due to the finite time step of the solver. The Shampine-Reichelt-Kierzenka method (ode23t) is artifact-free, even in the extremities of steepest increase in V. However, all simulations show that the trajectory does not superpose, a signature of aperiodicity. Note that, despite the dramatic differences in the $\dot{V}$ dimension, the range of V is identical.

References

[1] Feynman, Leighton and Sands. The Feynman Lectures in Physics. Addison-Wesley (1965)

[2] Barabasi. Scale-Free Networks: A Decade and Beyond. *Science* **325** (5939) pp. 412 (2009)

[3] Makarov et. al. A method for determining neural connectivity and inferring the underlying network dynamics using extracellular spike recordings. *Journal of Neuroscience Methods* **144** pp. 265–279 (2005)

[4] Liu et. al. A model neuron with activity-dependent conductances regulated by multiple calcium sensors. *Journal of Neuroscience* **18** (7) pp.2309–2320 (1998)

[5] Prinz et. al. Alternative to hand-tuning conductance-based models: construction and analysis of Databases of Model Neurons. *Journal of Neurophysiology* **90** pp. 3998-4015 (2003)

[6] Elliot et. al. An invariance principle for maintaining the operating point of a neuron. *Network: Computation in Neural Systems* **19** (3) pp. 213–235 (2008)

[7] Timme et. al. Coexistence of regular and irregular dynamics in complex networks of pulse-coupled Oscillators. *Physical Review Letters* **89** (25) pp. 258701 (2002)

[8] Memmesheimer and Timme. Designing complex networks. *Physica D: Nonlinear Phenomena* **224** (1-2) pp. 182-201 (2006)

[9] Memmesheimer and Timme. Designing the dynamics of spiking neural networks. *Physical Review Letters* **97** (18) pp. 188101 (2006)

[10] Bang-Jensen and Gutin. Digraphs: Theory, Algorithms and Applications. Springer, pp. 1-772 (2007)

[11] Timme. Does dynamics reflect topology in directed networks? *Europhysics Letters* **76** (3) pp. 367–373 (2006)

REFERENCES

[12] Dharmadi and Gonzalez. Elementary network reconstruction: A framework for the analysis of regulatory networks in biological systems. *Journal of Theoretical Biology* doi:10.1016/j.jtbi.2009.12.007 (2009)

[13] Liu and Buonomano. Embedding Multiple Trajectories in Simulated Recurrent Neural Networks in a Self-Organizing Manner. *Journal of Neuroscience* **29** (42) pp. 13172 (2009)

[14] Kori and Mikhailov. Entrainment of randomly coupled oscillator networks by a pacemaker. *Physical Review Letters* **93**, 254101 (2004)

[15] Goaillard et. al. Functional consequences of animal-to-animal variation in circuit parameters. *Nature Neuroscience* **12** (11) pp. 1424-1430 (2009)

[16] Goldman et. al. Global structure, robustness, and modulation of neuronal models. *Journal of Neuroscience* **21** (14) pp.5229–5238 (2001)

[17] Diestel. Graph Theory. Birkhauser, pp. 1-422 (2005)

[18] Bondy and Murty. Graph theory with Applications. Springer, pp. 1-270 (2008)

[19] Gerstner and Naud. How Good Are Neuron Models? *Science* **326** (5951) pp. 379 (2009)

[20] Kim et. al. Inferring gene regulatory networks from temporal expression profiles under time-delay and noise. *Computational biology and chemistry* **31** pp. 239–245 (2007)

[21] Gardner et. al. Inferring genetic networks and identifying compound mode of action via expression profiling. *Science,* **301** pp. 102-105 (2003)

[22] Guimera and Sales-Pardo. Missing and spurious interactions and the reconstruction of complex networks. *Proceedings of the National Academy of Sciences* **106** (52) pp. 22073-22078 (2009)

[23] Kramer et. al. Network inference with confidence from multivariate time series. *Physical Review E* **79** (6) p. 061916 (2009)

[24] Selverston et. al. Neural mechanisms underlying the generation of the lobster gastric mill motor pattern. *Frontiers in Neural Circuits* pp. 1-37 (2009)

[25] Hartmann and Weigt. Phase Transitions in Combinatorial optimisation Problems. Wiley-VCH Verlag GmbH & Co. pp. 1-45. (2008)

[26] Strogatz. From Kuramoto to Crawford: exploring the onset of synchronization in populations of coupled oscillators. *Physica D: Nonlinear Phenomena* **143** pp. 1–20 (2000)

[27] Zanette. Propagation of small perturbations in synchronized oscillator networks. *Europhysics Letters* http://arXiv.org/abs/cond-mat/0409159v1 (2004)

[28] Timme. Revealing Network Connectivity from Response Dynamics. *Physical Review Letters* **98** (22) pp. 4-6 (2007)

[29] Tegner et. al. Reverse engineering gene networks: Integrating genetic perturbations with dynamical modeling. *Proceedings of the National Academy of Sciences* **100** (10) pp. 5944 –5949 (2003)

[30] Turrigiano et. al. Selective regulation of current densities underlies spontaneous changes in the activity of cultured neurons. *Journal of Neuroscience* **15** (5) pp. 3640-3652 (1995)

[31] Foster et. al. Significance of conductances in Hodgkin-Huxley models. *Journal of Neurophysiology* **70** (6) pp. 2501-2517 (1993)

[32] Prinz et. al. Similar network activity from disparate circuit parameters. *Nature Neuroscience* **7** (12) pp. 1345-1352 (2004)

[33] Arenas et. al. Synchronization reveals topological scales in complex networks. *Physical Review Letters* **96**, 114102 (2006)

[34] Acebron et. al. The Kuramoto model: a simple paradigm for synchronization phenomena. *Reviews of Modern Physics*, **77** (1) pp. 137-185 (2005)

[35] Prinz. et al. The Functional Consequences of Changes in the Strength and Duration of Synaptic Inputs to Oscillatory Neurons. *Journal of Neuroscience* **23** (3) pp.943–954 (2003)

[36] Dayan and Abbott. Theoretical Neuroscience. (2007)

[37] Schulz et. al. Variable channel expression in identified single and electrically coupled neurons in different animals. *Nature Neuroscience* **9** (3) pp. 356-362 (2006)

[38] Denker et. al. A Network of Electronic Neural Oscillators Reproduces the Dynamics of the Periodically Forced Pyloric Pacemaker Group. *IEEE Transactions on Biomedical Engineering* **52** (5) pp. 782-798 (2005)

[39] Shampine et. al. Solving Index-1 DAEs in MATLAB and Simulink. *SIAM Review*, **41**. pp 538-552. (1999)

[40] Wilson. Consilience. Knopf, New York. p.85 (1998).

REFERENCES

[41] Strogatz. Exploring complex networks. *Nature* **410** pp. 268-269 (2001)

[42] Southgate. *God, Humanity, and the Cosmos*. 2nd edition. T&T Clark International pp. 122-125. (2005)

[43] Harris-Warrick, et. al. Dynamic Biological Networks. The Stomatogastric Nervous System (MIT Press, Cambridge, Massachusetts, USA, 1992).

[44] Turrigiano et. al. Selective regulation of current densities underlies spontaneous changes in the activity of cultured neurons. *Journal of Neuroscience.* **15**, 3640–3652 (1995).

[45] Abbott. and Marder. Modeling Small Networks. in *Methods in Neuronal Modeling: From Ions to Networks* (eds. Koch, C. & Segev, I.) 361–410 (MIT Press, Cambridge, 1998).

[46] Marder. Cholinergic motor neurones in the stomatogastric system of the lobster. *Journal of Physiology* (London) **257**, 63–86 (1976).

[47] Selverston, Russell, Miller, and King. The stomatogastric nervous system: structure and function of a small neural network. *Prog. Neurobiol.* **7**, 215–290 (1976).

[48] Marder and Eisen. Transmitter identification of pyloric neurons: electrically coupled neurons use different neurotransmitters. *Journal of Neurophysiology* **51**, 1345–1361 (1984).

[49] Eisen and Marder. Mechanisms underlying pattern generation in lobster stomatogastric ganglion as determined by selective inactivation of identified neurons. *Journal of Neurophysiology* **48**, 1392–1415 (1982).

[50] Strogatz. Sync: The Emerging Science of Spontaenous Order. Hyperion Books, (2003)

[51] Milgram. The Small World Problem. *Psychology Today*, **1** (1), pp. 61-67 (1967)

[52] Milgram et. al. The lost-letter technique: A tool of social research. *The Public Opinion Quarterly* **29** (3) pp. 437-438 (1965)

[53] Watts and Strogatz. Collective Dynamics of 'Small-World' Networks. *Nature* **393**, pp. 440- 444 (1998)

[54] Sporns and Honey. Small Worlds inside Big Brains. *Proceedings of the National Academy of Sciences.* **103** (51) pp. 19219 –19220 (2006)

[55] Sporns and Zwi. The Small World of the Cerebral Cortex. *Neuroinformatics* **4**, pp. 145–162 (2004)

[56] Bostrom. A History of Transhumanist Thought. *Journal of Evolution and Technology* **14** (1). (2005)

[57] Bostrom. When machines outsmart humans. *Futures.* **35** (7) pp. 759-764. (2003)

[58] Kurzweil. The Singularity is Near: When Humans Transcend Biology. Penguin Press. (2005)

[59] Kandel et. al. Principles of Neural Science. McGraw-Hill. (2000)